

# Pairing at a single Van Hove point

Risto Ojajarvi,<sup>1</sup> Andrey V. Chubukov,<sup>2</sup> Yueh-Chen Lee,<sup>2</sup> Markus Garst,<sup>3,4</sup> and Jörg Schmalian<sup>1,4</sup>

<sup>1</sup>*Institut für Theorie der Kondensierten Materie,*

*Karlsruher Institut für Technologie; 76131 Karlsruhe, Germany*

<sup>2</sup>*W. I. Fine Theoretical Physics Institute, University of Minnesota, Minneapolis, MN 55455, USA*

<sup>3</sup>*Institut für Theoretische Festkörperphysik, Karlsruher Institut für Technologie; 76131 Karlsruhe, Germany*

<sup>4</sup>*Institut für QuantenMaterialien und Technologien,*

*Karlsruher Institut für Technologie; 76131 Karlsruhe, Germany*

We show that an interacting electronic system with a single ordinary or extended Van Hove point, which crosses the Fermi energy, is unstable against triplet superconductivity. The pairing mechanism is unconventional. There is no Cooper instability. Instead, pairing is due to the divergence of the density of states at a Van Hove point, leading to a superconducting quantum critical point at a finite detuning from the Van Hove point. The transition temperature is universally determined by the exponent governing the divergence of the density of states. Enhancing this exponent drastically increases  $T_c$ . The Cooper pair wave function has a non-monotonic momentum dependence with a steep slope near the gap nodes. In the absence of spin-orbit coupling, pairing fluctuations suppress a  $2e$  spin-triplet state, but allow pairs of triplets to condense into a charge- $4e$  singlet state at a temperature of similar order as our result.

## I. INTRODUCTION

The ability to create and manipulate two-dimensional (2D) or strongly anisotropic 3D electronic materials led to an increased interest in the theory of systems in which the Fermi energy is at or near a Van Hove (VH) singularity of the electronic density of states [1]. Examples are doped graphene[3–6], a wide range of moiré materials[7–13], metallic Kagome systems[14–16], as well as the ruthenate oxides  $\text{Sr}_3\text{Ru}_2\text{O}_7$  in an external magnetic field[17] and  $\text{Sr}_2\text{RuO}_4$  under uni-axial compressive strain [18–21]. Studies of these materials extended earlier theoretical analysis of VH singularities in cuprate and other superconductors [22–34].

In the analysis of the impact of VH singularities, two cases should be distinguished: In the first case, illustrated in Fig. 1(a), there are several symmetry-related VH points that simultaneously cross the Fermi energy. In this situation, scattering events with large transferred momentum that connect different VH points are crucial. These processes often lead to density-wave instabilities, which trigger superconductivity nearby in the phase diagram via some version of the Kohn-Luttinger mechanism [35–38]. In the second case, shown in Fig. 1(b), there is a single VH point at the Fermi level. Such a situation occurs in systems with low symmetry, including strained materials, where the application of large uni-axial stress reduces the number of allowed symmetry operations. A prominent example is  $\text{Sr}_2\text{RuO}_4$ , where stress along the Ru-O-Ru bond direction moves one of the VH points of the tetragonal system to the Fermi energy, while the other is pushed away from it [18–21].

In addition to ordinary VH points, where the density of states in 2D diverges like a logarithm, extended VH points have recently been discussed extensively[7–12]. In this case the density of states diverges by a power law due a saddle-point that is less dispersive than the ordinary quadratic one. In Refs. [8, 11] a classification of

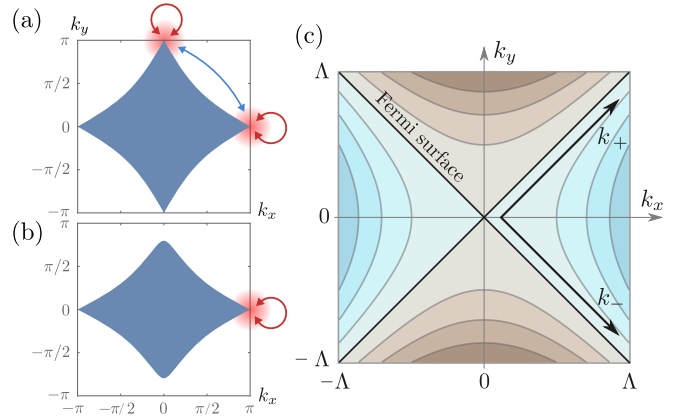


Figure 1. Fermi surface of a system with (a) two Van Hove points, and (b) a single Van Hove point at the Fermi energy. The shaded area shows the occupied states, and arrows illustrate the dominant interactions. (c) Iso-energy contours near the Van Hove point described by Eq. (4). Blue (brown) color indicates the occupied (unoccupied) states. The Fermi surface for the extended Van Hove point of Eq. (5) is the same, while the iso-energy contours will be different, with flatter bands near the Fermi energy. The coordinates  $k_{\pm} = (k_x \pm k_y)/\sqrt{2}$  are extensively used throughout the text, where we consider gap functions that depend on only one of these coordinates, i.e.  $\Delta(k_+)$  or  $\Delta(k_-)$ .

such extended singularities was given and it was shown that some extended VH points can be reached by solely varying a single parameter in the Hamiltonian.

For a single, ordinary or extended VH point, a Stoner-type analysis suggests a ferromagnetic instability at arbitrarily small interaction, due to the divergent density of states [13, 30]. However, no instability was detected in renormalization group (RG) studies [9, 12]. The authors of Ref. [9] argued, based on their RG study, that the ground state of a system with a single extended VH point is a particular non-Fermi liquid, dubbed a super-

metal, in which the quasi-particle weight vanishes by a power-law as one approaches low energies.

In this paper, we consider the behavior of a system of fermions with repulsive interaction and a single ordinary (extended) VH point in 2D with logarithmic (power-law) divergence of the density of states. We first present arguments in favor of the absence of a ferromagnetic Stoner instability and then demonstrate that the divergence in the density of states gives rise to odd-parity spin triplet superconductivity. To obtain such an instability we had to go beyond the conventional one-loop RG treatment, which accounts for the leading logarithms, but neglects the subleading ones. For an ordinary VH point, we obtain for the superconducting transition temperature

$$T_c = T_0 \exp\left(-\frac{1 + \mu g}{\gamma g}\right). \quad (1)$$

Here,  $g$  is the dimensionless coupling constant to be defined below,  $\gamma$  and  $\mu$  are of order one, and  $T_0 = \frac{\Lambda^2}{2m}$ , where  $m$  is the curvature of the quadratic saddle-point dispersion around a VH point and  $\Lambda$  is the upper momentum cutoff of the theory. For an extended VH point we obtain

$$T_c \sim T_0 g^{\frac{1+\epsilon}{2\epsilon}}, \quad (2)$$

where  $\epsilon$  is the exponent that determines the divergence of the density of states,  $\rho(\omega) \propto |\omega|^{-\epsilon}$ .  $T_c$  of an extended Van Hove point is no longer exponentially small and gets strongly enhanced when  $\epsilon$  increases. Furthermore, we show that this  $T_c$  is cutoff-independent as the dependence on  $\Lambda$  cancels out between  $T_0$  and  $g$ . Our result indicates that the supermetal of Ref. [9] describes the normal state over some temperature and energy range, but at lowest temperatures or energies the system eventually becomes unstable against triplet superconductivity.

Solving the gap equation for  $T \lesssim T_c$ , we find that the pairing state is highly non-local with an unusual momentum dependence of the Cooper-pair wave function. It changes sign under  $\mathbf{k} \rightarrow -\mathbf{k}$  as required for odd-parity triplet pairing. However, the momentum regime, where the gap is linear in  $\mathbf{k}$ , turns out to be extremely small, of order  $\delta k \sim 2mT_c/\Lambda$  in the case of an ordinary VH point. Nodal excitations should therefore be hardly visible in thermodynamic measurements such as the specific heat, the Knight shift or the superfluid stiffness.

We also analyze the role of pairing fluctuations. The results Eqs. (1) and (2) are mean-field transition temperatures. For a spin-singlet superconductor, the actual transition at  $T_{\text{BKT}} \leq T_c$  is of Berezinskii-Kosterlitz-Thouless (BKT) type [50, 51] into a charge- $2e$  state with algebraic order (power-law decay of superconducting correlations). For a 2D spin-triplet state, a charge- $2e$  order survives in the presence of spin-orbit interaction. In its absence a spin-triplet order is additionally suppressed by fluctuations in the spin sector of the superconducting order parameter [52, 53]. However, there exists a BKT transition into to a charge- $4e$  state, in which two triplets

bind into a singlet. In either case, the onset temperature for the algebraic superconductivity is comparable to the mean-field  $T_c$ , given in Eqs. (1) and (2).

## II. THE MODEL

We consider a system of interacting electrons with dispersion  $\varepsilon_{\mathbf{k}}$  and Hubbard repulsion  $U$ :

$$H = \sum_{\mathbf{k}\alpha} \varepsilon_{\mathbf{k}} \psi_{\mathbf{k}\alpha}^\dagger \psi_{\mathbf{k}\alpha} + \frac{U}{N} \sum_{\mathbf{k}\mathbf{k}'\mathbf{q}\alpha\beta} \psi_{\mathbf{k}\alpha}^\dagger \psi_{\mathbf{k}'\beta}^\dagger \psi_{\mathbf{k}'-\mathbf{q}\beta} \psi_{\mathbf{k}+\mathbf{q}\alpha}, \quad (3)$$

where  $\psi_{\mathbf{k}\alpha}$  annihilates an electron with momentum  $\mathbf{k}$  and spin  $\alpha$ . We measure the momenta relative to the VH point, assumed to be time-reversal symmetric, and focus on the case where  $\varepsilon_{\mathbf{k}=\mathbf{0}} = 0$ , i.e., the VH point is right at the Fermi level. In the last section, we comment on the behavior upon tuning the Fermi energy away from the VH point.

For an ordinary VH point the electronic dispersion is

$$\varepsilon_{\mathbf{k}} = \frac{1}{2m} (k_x^2 - k_y^2). \quad (4)$$

An anisotropy between  $k_x$  and  $k_y$ , expected for a VH point located away from the center of the Brillouin zone, can be eliminated by an appropriate re-scaling of momenta. The quadratic dispersion in Eq. (4) gives rise to a logarithmically diverging density of states  $\rho(\omega) \sim m \log\left(\frac{\Lambda^2}{m|\omega|}\right)$ , where  $\Lambda$  is the momentum cutoff – the highest momentum, up to which Eq. (4) is valid.

For an extended VH point, we follow earlier works [27, 29, 31, 32] and consider the dispersion in the form

$$\varepsilon_{\mathbf{k}} = A (|k_x|^n - |k_y|^n), \quad (5)$$

where  $n \geq 2$ . Now the density of states diverges by a power-law  $\rho(\omega) \sim A^{\epsilon-1} |\omega|^{-\epsilon}$  with  $\epsilon = 1 - 2/n \geq 0$ . In this paper, we focus on the dispersion Eq. (5), but note that other extended VH singularities are possible, e.g., with different powers for the two components of  $\mathbf{k}$  [7–12].

## III. A POTENTIAL STONER INSTABILITY

We begin with the discussion of a potential instability towards ferromagnetism. At a first glance, ferromagnetism near a single VH point is a natural option [30], as this is a  $\mathbf{q} = 0$  instability, and it develops for a repulsive interaction between fermions. Within the random phase approximation (RPA), the instability occurs when the dimensionless interaction – the product of  $U$  and the density of states – reaches a certain finite value. In standard situations, this requires that the interaction strength exceeds a threshold value. For the VH case, however, the density of states is divergent, and within RPA the Stoner

condition is satisfied already for an arbitrarily weak interaction.

Whether or not a Stoner instability develops beyond RPA can be detected by computing the static and uniform magnetic susceptibility  $\chi$ , i.e. the limit  $\mathbf{q} \rightarrow 0$  of the static susceptibility  $\chi(\mathbf{q}, \omega = 0)$ . This susceptibility can be obtained by either introducing an infinitesimal magnetic field and computing the magnetization or by introducing an infinitesimal bare ferromagnetic order parameter, dressing it by interactions, and computing the ratio of the fully-dressed and the bare order parameters. In the diagrammatic analysis, the second approach is easier to implement. The bare order parameter  $M_0$  is represented as a two-particle vertex, and the dressed one  $M$  is obtained by renormalizing this vertex by interactions. This is illustrated in Fig. 2(a).

For definiteness, we consider a single ordinary VH point. The particle-hole polarization bubble at a VH point is  $\Pi_{\text{ph}} = \frac{m}{2\pi^2} \log \frac{T_0}{T}$  with  $T_0$  given below Eq. (1). Summing up ladder (RPA) series of particle-hole renormalizations of  $M_0$  one obtains

$$M = M_0 \left( 1 + U\Pi_{\text{ph}} + (U\Pi_{\text{ph}})^2 + \dots \right) = \frac{M_0}{1 - U\Pi_{\text{ph}}}. \quad (6)$$

The susceptibility  $M/M_0$  diverges at  $U\Pi_{\text{ph}} = 1$ , i.e., at  $T = T_{\text{FM}}$  satisfying  $\lambda_0 \log \frac{T_0}{T_{\text{FM}}} = 1$ , where

$$\lambda_0 = \frac{mU}{2\pi^2}. \quad (7)$$

The ferromagnetic transition temperature  $T_{\text{FM}}$  is finite no matter how small  $U$  is.

This analysis, however, does not hold beyond RPA, once we include crossed diagrams (Fig. 2(c)), which represent insertions of particle-particle renormalizations into the particle-hole channel. At zero total momentum, a particle-particle polarization bubble  $\Pi_{\text{pp}} = \frac{m}{2\pi^2} \log^2 \frac{T_0}{T}$  diverges as  $\log^2$  due to an additional Cooper logarithm. If we use this expression and add the ladder series of particle-particle renormalizations to each term in Eq. (6), we effectively replace  $U$  by

$$\begin{aligned} U_{\text{eff}} &= U \left( 1 - U\Pi_{\text{pp}} + U^2\Pi_{\text{pp}}^2 \dots \right) \\ &= \frac{U}{1 + \lambda_0 \log^2 \frac{T_0}{T}}. \end{aligned} \quad (8)$$

Substituting  $U_{\text{eff}}$  instead of  $U$  into Eq. (6), we find that the Stoner condition becomes

$$\frac{\lambda_0 \log \frac{T_0}{T_{\text{FM}}}}{1 + \lambda_0 \log^2 \frac{T_0}{T_{\text{FM}}}} = 1. \quad (9)$$

We show in Appendix A that the same result is obtained by using a renormalization group analysis with flow parameter  $l = \log^2 \frac{\Lambda}{k}$ . There is no solution of Eq. (9) at small  $\lambda_0$  because the suppression of  $\lambda_0$  by fluctuations in the particle-particle channel is stronger than the enhancement of  $\lambda_0$  in the particle-hole channel.

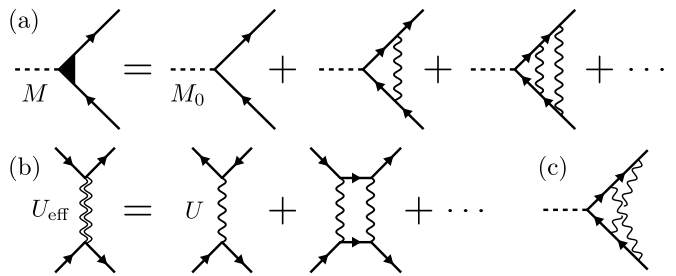


Figure 2. Diagrammatic representation of the fully-dressed order parameter  $M$  in terms of the infinitesimally small bare one  $M_0$ . (a) Ladder series in the particle-hole channel [Eq. (6)]. (b) Series of particle-particle diagrams [Eq. (8)] which renormalize the interaction. (c) A diagram, generated by inserting a particle-particle renormalization into the particle-hole ladder series. At a Stoner transition, the diagrammatic series from  $M/M_0$  must sum to infinity; see text for further details.

This reasoning is, however, imprecise as it assumes that one can use  $\Pi_{\text{pp}} \propto \log^2 T_0/T$  in a situation when the total momentum of the two intermediate fermions in the crossed diagram is non-zero. We have explicitly evaluated the renormalization of  $U$  from the two-loop crossed diagram in Fig.2(c) and found

$$U_{\text{eff}} = U \left( 1 - b\lambda_0 \log \frac{T_0}{T} \right), \quad (10)$$

where  $b \approx 1.88$ . The details of this analysis are summarized in Appendix A, where we determine the coefficient  $b$  numerically and show analytically that the naively expected  $\log^2 \frac{T_0}{T}$  contribution vanishes due to a cancellation of different terms that individually scale as  $\log^2 \frac{T_0}{T}$ .

It is *a-priori* unclear how to re-sum the diagrams for  $U_{\text{eff}}$  and whether it is even justified to restrict to maximally crossed diagrams. If we assume that higher-order crossed diagrams form a geometrical series, we find  $U_{\text{eff}} = U/(1 + b\lambda_0 \log(T_0/T))$ , which replaces Eq. (9) for the condition for the Stoner instability by

$$\frac{\lambda_0 \log \frac{T_0}{T}}{1 + \lambda_0 b \log \frac{T_0}{T}} = 1. \quad (11)$$

Since  $b > 1$ , one still finds that there is no Stoner instability. This argument is, however, a suggestive one, and whether there is a Stoner instability at a single VH point remains an open question. In what follows, we will assume that no ferromagnetic instability takes place and analyze a potential pairing instability.

#### IV. PAIRING INSTABILITY

We now show that there is a pairing instability for the cases of both, the ordinary and the extended VH point. In order to theoretically detect it one has to go beyond the usual one-loop renormalization group treatment and

include not only the leading logarithms, which cancel out, as we will see, but also the subleading ones. We will show that the pairing mechanism in our case is of the Kohn-Luttinger type, but is nevertheless different from the conventional Kohn-Luttinger scenario. In the latter, the screening of a repulsive Hubbard-type interaction  $U$  generates an attractive pairing interaction in the spin-triplet channel with dimensionless coupling constant

$$g \equiv \lambda_0^2 = \frac{m^2 U^2}{4\pi^4}, \quad (12)$$

which gives rise to a BCS-type pairing instability. For an ordinary VH point, this would give rise to  $T_c \sim T_0 e^{-1/\sqrt{g}}$  originating from  $g \log^2(T_0/T_c) = 1$ , where one logarithm is a Cooper one and the other is due to the VH singularity in the density of states; we remind that  $T_0$  was introduced below Eq. (1). Such a result holds for a Fermi surface without VH points when the attractive pairing interaction is a logarithmically singular function of the frequency transfer[39, 40]. In our case, the attraction in the spin-triplet channel does appear due to screening by particle-hole pairs and is of order  $U^2$ . However, the effective pairing interaction  $\Gamma_{\alpha\beta\gamma\delta}(\mathbf{k}, -\mathbf{k}, \mathbf{p}, -\mathbf{p})$ , where  $\mathbf{k}$  and  $\mathbf{p}$  are relative to the VH point, is strongly momentum dependent in the triplet channel and is reduced when one momentum is much smaller than the other one. This effectively eliminates the Cooper logarithm leaving only the one from the density of states. As a result, we will find that  $T_c$  is given by Eq. (1). The same holds for a higher-order VH point. In this case, there is no exponential dependence of  $T_c$  on  $g$  but  $T_c$  is still reduced compared to that in the conventional Kohn-Luttinger scenario.

A generic recipe for the analysis of potential pairing mediated by nominally repulsive electron-electron interaction is to consider an irreducible pairing vertex

$$\Gamma_{\alpha\beta\gamma\delta}(\mathbf{k}, \mathbf{p}) = \Gamma_{\alpha\beta\gamma\delta}(\mathbf{k}, -\mathbf{k}, \mathbf{p}, -\mathbf{p}) \quad (13)$$

instead of the bare  $U$  because  $\Gamma$  rather than  $U$  appears in the gap equation [46]. The irreducible pairing vertex is the anti-symmetrized interaction with zero total incoming and outgoing momenta, dressed by the renormalizations outside of the particle-particle channel, i.e. by processes which in a diagrammatic representation have no cross-sections with two fermionic propagators with opposite momenta. To second order in  $U$ , the static irreducible vertex takes the form [60]

$$\begin{aligned} \Gamma_{\alpha\beta\gamma\delta}(\mathbf{k}, \mathbf{p}) &= U(\delta_{\alpha\beta}\delta_{\gamma\delta} - \delta_{\alpha\delta}\delta_{\beta\gamma}) \\ &+ U^2 \Pi_{\text{ph}}(\mathbf{k} + \mathbf{p}) \delta_{\alpha\beta}\delta_{\gamma\delta} \\ &- U^2 \Pi_{\text{ph}}(\mathbf{k} - \mathbf{p}) \delta_{\alpha\delta}\delta_{\beta\gamma}. \end{aligned} \quad (14)$$

The underlying processes are shown in Fig. 3, where  $\Pi_{\text{ph}}(\mathbf{k})$  is the static particle-hole polarization bubble.

The restriction to second order in  $U$  may seem questionable as in the previous section we argued that the coupling in the particle-hole channel is reduced, to the

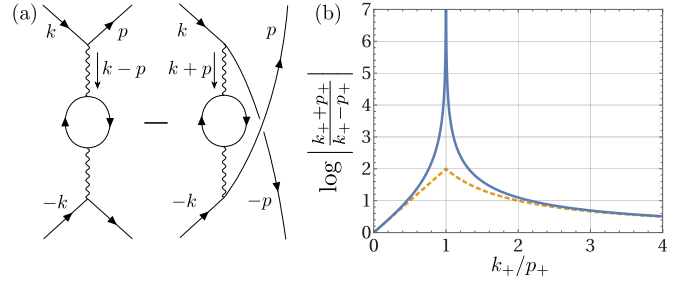


Figure 3. (a) Pairing interaction  $\Gamma_{\alpha\beta\gamma\delta}(\mathbf{k}, \mathbf{p})$  of Eq. (14) at second order in  $U$ , dressed by particle-hole excitations. Solid lines stand for fermions, which give rise to the bubble  $\Pi_{\text{ph}}$ . The wiggly line stands for the local interaction  $U$ . (b) The function  $\log \left| \frac{k_+ + p_+}{k_+ - p_+} \right|$ , which determines the triplet component of  $\Gamma_{\alpha\beta\gamma\delta}(\mathbf{k}, \mathbf{p})$  for  $k_- = p_- = 0$ , as a function of  $k_+ / p_+$ . The interaction gets weak whenever one of the two momenta is small. The blue solid line is the actual function, while the orange dashed line is an approximate expression based on Eq. (28).

extent that no Stoner instability takes place. We will show, however, that the typical momenta  $\mathbf{k}$  and  $\mathbf{p}$ , responsible for pairing, are comparable to the cutoff  $\Lambda$ . For such momenta, the suppression of the coupling by crossed diagrams is small and can be neglected.

### A. Pairing at the ordinary VH point

The gap equation for the ordinary VH point takes the conventional form

$$\Delta_{\alpha\beta}(\mathbf{k}) = - \int_{\mathbf{p}} \frac{\tanh\left(\frac{\varepsilon_{\mathbf{p}}}{2(1+Z_{\mathbf{p}})T}\right) \Gamma_{\alpha\gamma\beta\delta}(\mathbf{k}, \mathbf{p})}{2\varepsilon_{\mathbf{p}}(1+Z_{\mathbf{p}})} \Delta_{\gamma\delta}(\mathbf{p}). \quad (15)$$

Here  $Z_{\mathbf{p}}$  is the inverse quasi-particle weight, related to the fermionic self-energy by  $\Sigma(\mathbf{k}, \omega) = -i\omega Z_{\mathbf{k}}$ . It is convenient to rotate the coordinate system by  $\pi/4$  and introduce  $k_{\pm} = \frac{1}{\sqrt{2}}(k_x \pm k_y)$  and  $p_{\pm} = \frac{1}{\sqrt{2}}(p_x \pm p_y)$ . The Fermi surface around a VH point is specified by either  $p_+ = 0$  or  $p_- = 0$ , see Fig. 1(c). In these notations [33, 34]

$$Z_{\mathbf{p}} = 2g \log(2) \log \frac{\Lambda}{|p_+|} \log \frac{\Lambda}{|p_-|}, \quad (16)$$

The gap equation can be split into two decoupled equations for the singlet and triplet components, respectively, by expressing the gap function as

$$\Delta_{\alpha\beta}(\mathbf{k}) = \Delta_s(\mathbf{k}) i\sigma_{\alpha\beta}^y + \mathbf{\Delta}(\mathbf{k}) \cdot (i\sigma^y \boldsymbol{\sigma})_{\alpha\beta}. \quad (17)$$

The bare interaction  $U$  shows up only in the singlet channel, the dressed  $\Gamma_{\alpha\beta\gamma\delta}(\mathbf{k}, \mathbf{p})$  of Eq. (14) has both, singlet and triplet components. One easily finds that there is no solution for  $\Delta_s(\mathbf{k})$  in the singlet channel, because the

dressed pairing vertex remains repulsive. In the triplet channel, the gap equation takes the form

$$\begin{aligned} \Delta_i(\mathbf{k}) &= -U^2 \int_{\mathbf{p}} \frac{\tanh\left(\frac{\varepsilon_{\mathbf{p}}}{2(1+Z_{\mathbf{p}})T}\right)}{2\varepsilon_{\mathbf{p}}(1+Z_{\mathbf{p}})} \Delta_i(\mathbf{p}) \\ &\times (\Pi_{\text{ph}}(\mathbf{k}+\mathbf{p}) - \Pi_{\text{ph}}(\mathbf{k}-\mathbf{p})), \end{aligned} \quad (18)$$

with  $i = x, y, z$ . In what follows we choose an arbitrary quantization axis in spin space and drop the index  $i$ . We get back to this issue when we discuss superconducting fluctuations.

In terms of  $k_{\pm}$  and  $p_{\pm}$  the pairing vertex is the sum of two terms

$$\begin{aligned} &\Pi_{\text{ph}}(\mathbf{k}+\mathbf{p}) - \Pi_{\text{ph}}(\mathbf{k}-\mathbf{p}) \\ &= \frac{m}{2\pi^2} \left( \log \frac{|k_+ - p_+|}{|k_+ + p_+|} + \log \frac{|k_- - p_-|}{|k_- + p_-|} \right). \end{aligned} \quad (19)$$

We see that one of the terms vanishes when either  $k_+ = 0$  or  $k_- = 0$ . This allows to search for  $\Delta(\mathbf{k})$  which depends only on one of the coordinates, i.e.,  $\Delta(k_+)$  or  $\Delta(k_-)$ . Even if there exist more complicated solutions, finding a solution of this kind is enough to establish a lower bound for the superconducting  $T_c$ . For definiteness, below we consider  $\Delta(\mathbf{k}) = \Delta(k_+)$  and  $\Delta(\mathbf{p}) = \Delta(p_+)$ . Under this assumption we can perform the integration over  $p_-$  at the outset and obtain

$$\int_{-\Lambda}^{\Lambda} \frac{dp_-}{2\pi} \frac{\tanh\left(\frac{p_+ p_-}{2mT}\right)}{\frac{2p_+ p_-}{m}(1+Z_{\mathbf{p}})} = \frac{m}{2\pi|p_+|} K(p_+). \quad (20)$$

The function

$$K(p_+) \approx \frac{\log\left(1 + 2g \log(2) \log \frac{\Lambda}{p_+} \log \frac{p_+ \Lambda}{2mT}\right)}{2g \log(2) \log \frac{\Lambda}{p_+}} \quad (21)$$

determines the effective density of states for momenta transverse to the Fermi surface. The expression is valid when  $\frac{p_+ \Lambda}{2mT} \gg 1$ , setting the temperature dependent lower cutoff for  $p_+$  at  $2mT/\Lambda$ . The upper cutoff is at  $p_+ = \Lambda$ . For  $g \rightarrow 0$ ,  $K(p_+) \rightarrow \log \frac{p_+ \Lambda}{2mT}$ .

It is convenient to introduce dimensionless variables  $\bar{p} = \frac{\Lambda p_+}{2mT}$  and similar for  $\bar{k}$ , and  $\bar{\Lambda} = \frac{\Lambda^2}{2mT}$ . In these variables the gap equation takes the form

$$\Delta(\bar{k}) = -g \int_1^{\bar{\Lambda}} \frac{d\bar{p}}{\bar{p}} K(\bar{p}) \log \left| \frac{\bar{k} - \bar{p}}{\bar{k} + \bar{p}} \right| \Delta(\bar{p}), \quad (22)$$

with

$$K(\bar{p}) = \frac{\log\left(1 + 2g \log(2) \log\left(\frac{\bar{\Lambda}}{\bar{p}}\right) \log \bar{p}\right)}{2g \log(2) \log\left(\frac{\bar{\Lambda}}{\bar{p}}\right)}. \quad (23)$$

We solved this equation numerically and obtained  $T_c(g)$  and  $\Delta(\bar{k})$ . In Fig. 4 we plot  $gY(g)$  with

$$Y(g) \equiv \log \frac{T_0}{T_c} \quad (24)$$

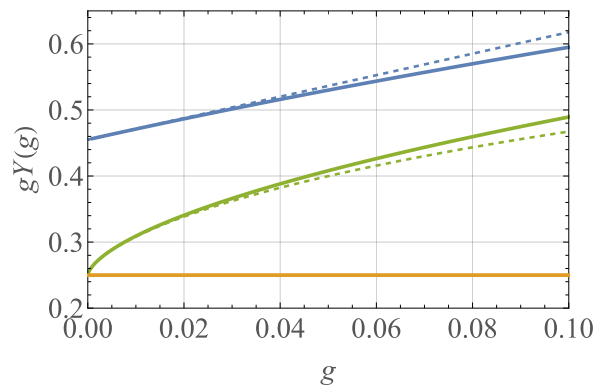


Figure 4. Variation of  $gY(g) = g \log \frac{T_0}{T_c(g)}$  with the dimensionless coupling constant  $g$ . Blue curves are the full solution of the linearized gap equation (22) with self-energy included. The blue dashed line is a fit to  $(1 + \mu g)/\gamma$  with  $\gamma$  and  $\mu$  given in Eq. (25). This dependence of  $gY(g)$  leads to Eq. (1) for  $T_c(g)$ . The green lines are the solutions of the gap equation without self-energy, which we discuss in section IV A 2. The solid green line is the full numerical solution while the dashed line is the analytic solution of an approximate Eq. (46). The orange line is the zero-order approximate result, Eq. (36). Recall that larger  $Y(g)$  correspond to smaller  $T_c$ .

as function of the coupling constant  $g$ . We find that at small  $g$  the behavior is well described by a linear relation  $g \log \frac{T_0}{T_c} = (1 + \mu g)/\gamma$  with

$$\begin{aligned} \gamma &\approx 2.197 \\ \mu &\approx 3.515. \end{aligned} \quad (25)$$

This yields the transition temperature given in Eq. (1). In Fig. 5 we show the momentum dependence of the gap function  $\Delta(\bar{k})$  extracted from the numerical solution.  $\Delta(\bar{k})$  is odd under  $\bar{k} \rightarrow -\bar{k}$  as required for an odd-parity triplet state. The momentum dependence is non-monotonic with a maximum at an intermediate momentum, which scales with  $\Lambda$  but numerically is much smaller than  $\Lambda$ . The linear dependence of  $\Delta(\bar{k})$  on  $\bar{k}$  holds at even smaller momenta below the maximum.

To gain physical insight and better interpret our numerical findings, we next perform an analytic analysis of the gap equation. We obtain two approximate solutions, which qualitatively reproduce the full numerical one and provide transparent insights into the key aspects of the pairing instability.

#### 1. An approximate analytical solution assuming a constant density of states

We begin by analyzing the gap equation under the simplifying assumption that relevant  $\bar{p}$  are of order  $\bar{\Lambda}$  ( $p_+ \sim \Lambda$ ). In this situation, one can expand Eq. (21) in  $g$  and obtain a momentum-independent density of states  $K(p_+) \approx \log \bar{\Lambda}$ , which can be pulled out of the integral

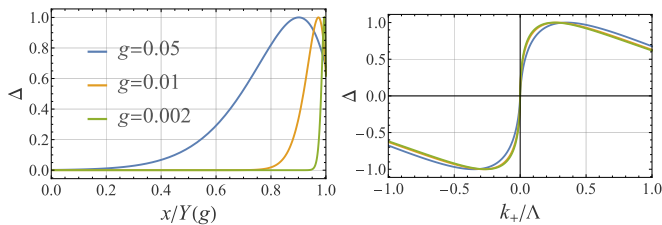


Figure 5. Momentum dependence of the superconducting gap function, obtained from the solution of the linearized gap equation (22) with effective density of states  $K(\bar{p})$  given by Eq. (23). Such a gap function develops infinitesimally below  $T_c$ . The gap function is normalized to its maximal value. Left panel:  $\Delta(x)$  as a function of  $x/Y(g)$ , where  $x = \log\left(\frac{\Lambda k_+}{2mT}\right)$  and  $Y(g) = \log T_0/T_c(g)$ . Right panel:  $\Delta(k_+)$  as function of  $k_+/\Lambda$ . Notice the non-monotonic behavior of the gap function with a steep slope at small momenta.

over  $\bar{p}$  in Eq. (22). The gap equation then reduces to

$$\Delta(\bar{k}) = g^* \int_1^{\bar{\Lambda}} \frac{d\bar{p}}{\bar{p}} \log \left| \frac{\bar{k} + \bar{p}}{\bar{k} - \bar{p}} \right| \Delta(\bar{p}), \quad (26)$$

with effective coupling constant

$$g^* = g \log \bar{\Lambda}. \quad (27)$$

As a further simplification, we follow Refs. [40, 41] and split the integral over  $\bar{p}$  into the regimes  $\bar{p} < \bar{k}$  and  $\bar{p} > \bar{k}$  and in each regime approximate

$$\log \left| \frac{\bar{k} - \bar{p}}{\bar{k} + \bar{p}} \right| \approx \begin{cases} -2\frac{\bar{p}}{\bar{k}} & \text{if } \bar{p} \ll \bar{k} \\ -2\frac{\bar{k}}{\bar{p}} & \text{if } \bar{k} \ll \bar{p} \end{cases}. \quad (28)$$

We then obtain

$$\Delta(\bar{k}) = 2g^* \left[ \frac{1}{\bar{k}} \int_1^{\bar{k}} d\bar{p} \Delta(\bar{p}) + \bar{k} \int_{\bar{k}}^{\bar{\Lambda}} \frac{d\bar{p}}{\bar{p}^2} \Delta(\bar{p}) \right]. \quad (29)$$

Differentiating w.r.t.  $\bar{k}$  we reduce Eq. (29) to a second order differential equation

$$\bar{k}^2 \Delta''(\bar{k}) + \bar{k} \Delta'(\bar{k}) + (4g^* - 1) \Delta(\bar{k}) = 0, \quad (30)$$

with UV and IR boundary conditions

$$\bar{\Lambda} \Delta'(\bar{\Lambda}) = -\Delta(\bar{\Lambda}), \quad (31)$$

$$\Delta'(1) = \Delta(1), \quad (32)$$

imposed by the original integral equation. For  $4g^* < 1$  (i.e., at higher temperatures), the solution of Eq. (30) is

$$\Delta(\bar{k}) = \Delta_0 \left( \bar{k}^{\sqrt{1-4g^*}} + e \bar{k}^{-\sqrt{1-4g^*}} \right), \quad (33)$$

where  $e$  is a free parameter. We verified that one cannot choose  $e$  to satisfy both boundary conditions. Hence, there is no solution for  $g^* < 1/4$ . For  $4g^* > 1$  the solution is

$$\Delta(k) = \Delta_0 \cos \left( \sqrt{4g^* - 1} \log k + \phi \right), \quad (34)$$

where  $\phi$  is a free parameter. The IR boundary condition specifies  $\phi$  to be the solution of  $\tan \phi = -(4g^* - 1)^{-1/2}$ , while the UV boundary condition yields

$$\sqrt{4g^* - 1} \log \bar{\Lambda} = l\pi - 2 \arctan \left( \sqrt{4g^* - 1} \right), \quad (35)$$

with integer  $l$ . Using  $\bar{\Lambda} = \Lambda^2/(2mT)$ , we find that this equation determines a discrete set of critical temperatures  $T_c(l)$ . The largest  $T_c$  corresponds to  $l = 1$  and is the solution of  $\sqrt{4g^* - 1} \approx \pi / \log \bar{\Lambda}$ . Solving at small  $g$ , we obtain

$$T_c \approx T_0 e^{-1/(4g)}. \quad (36)$$

This is similar to the expression given in Eq. (1), but with  $\gamma = 4$  and  $\mu = 0$ . This solution is the orange line in Fig. 4. While this approximation does not reproduce our numerical findings quantitatively, it does capture the two key features of the pairing instability of our problem. First, the Cooper logarithm is suppressed because the pairing interaction in Eq. (19) gets suppressed when an internal momentum is larger than an external one and vice versa. Taken alone, this suppression would impose a threshold value for pairing, i.e.  $T_c$  would be nonzero only for  $g$  larger than some critical value. Second, the large density of states, encoded in the phase space of transverse momenta that determine the function  $K(\bar{k})$  in Eq. (23), compensates for the weak pairing: it is the effective coupling constant  $g^* = g \log[\Lambda^2/(2mT)]$  of Eq. (27) that must reach a threshold. Because  $g^*(T \rightarrow 0) \rightarrow \infty$ , the threshold condition is satisfied at a finite  $T_c$  for any  $g$ . The combination of the two effects yields  $T_c$ , which has the same form as the BCS expression, albeit for a different reason.

There is a certain analogy between the solution for  $T_c$  and the gap function in our model and in the model with the singular dynamical interaction between fermions,  $\chi(\Omega_m) \propto 1/|\Omega_m|^\gamma$  (the  $\gamma$  model) [41–45]. In both cases, the integral equation for the gap function can be reduced to the differential equation with a marginal kernel, whose solution yields a power-law dependence of the gap function  $x^{\pm a}$  ( $x$  is a momentum in our case and a frequency in the  $\gamma$  model), where  $a$  depends on  $T$  in our case ( $a = \sqrt{1-4g^*}$ ) and on  $\gamma$  in the  $\gamma$ -model. As long as the exponent  $a$  is real the potential solution  $\Delta(x) = x^a + bx^{-a}$  does not satisfy the two boundary conditions, hence there is no superconductivity. A non-zero solution develops when the exponents  $\pm a$  merge. In this case, besides a constant, there appears the second solution  $\log x$ . The candidate solution  $\Delta(x) = 1 + b \log x$  satisfies the two boundary conditions, which fix the value of  $b$ , and hence is the actual solution of the linearized gap equation. This implies that  $a = 0$  is the condition for  $T_c$ . Also, in both cases the solution of the linearized gap equation exists even at  $4g^* > 1$ , as the end point of the infinite set of solutions of the non-linear gap equation.

## 2. Analytic solution for momentum-dependent density of states

We now advance to the next level and drop the assumption that the density of states  $K(p_+)$  can be approximated as momentum-independent. We still expand the density of states to first order in  $g$  (and, by doing this, neglect the self-energy), but keep  $K(\bar{p}) = \log \bar{p}$  instead of  $\log \bar{\Lambda}$  (we remind that  $\bar{p} = \frac{\Lambda p_+}{2mT}$ ). The gap equation takes the form

$$\Delta(\bar{k}) = -g \int_1^{\bar{\Lambda}} \frac{d\bar{p}}{\bar{p}} \log \bar{p} \log \left| \frac{\bar{k} - \bar{p}}{\bar{k} + \bar{p}} \right| \Delta(\bar{p}). \quad (37)$$

The lower momentum cutoff remains at  $\bar{p} = 1$ . We again split the integral over  $\bar{p}$  into the regions  $\bar{p} < \bar{k}$  and  $\bar{p} > \bar{k}$  and use Eq. (28). We then obtain

$$\Delta(\bar{k}) = 2g \int_1^{\bar{k}} \frac{d\bar{p}}{\bar{k}} \log \bar{p} \Delta(\bar{p}) + 2g\bar{k} \int_{\bar{k}}^{\bar{\Lambda}} \frac{d\bar{p}}{\bar{p}^2} \log \bar{p} \Delta(\bar{p}). \quad (38)$$

In logarithmic variables  $x = \log \bar{p}$  and  $y = \log \bar{k}$  this becomes

$$\Delta(y) = 2g \int_0^y dx x e^{x-y} \Delta(x) + 2g \int_y^Y dx x e^{y-x} \Delta(x), \quad (39)$$

where  $Y = \log \bar{\Lambda}$ . Differentiating twice over  $y$ , we find that (39) is equivalent to the second order differential equation

$$\frac{d}{dy} e^{-2y} \frac{d}{dy} e^y \Delta(y) = -4g e^{-y} \Delta(y), \quad (40)$$

with UV and IR boundary conditions:

$$\begin{aligned} \left. \frac{d\Delta}{dy} \right|_Y &= -\Delta|_Y, \\ \left. \frac{d\Delta}{dy} \right|_0 &= \Delta|_0. \end{aligned} \quad (41)$$

The differential equation (40) equals to

$$\Delta'' = (1 - 4gy) \Delta, \quad (42)$$

This last equation is equivalent to the Schrödinger equation in a linear potential  $V(y) = 1 - 4\lambda^2 y$  for zero eigenvalue,  $E = 0$ . The "coordinate" varies between  $y = 0$  and  $y = Y = \log \frac{\Lambda^2}{2mT}$ . If  $4\lambda^2 Y < 1$  the potential never becomes negative and getting a solution with zero eigenvalue is not possible. However, for  $4gY > 1$ , i.e.  $T < \frac{\Lambda^2}{2m} e^{-\frac{1}{4g}}$  a non-zero solution becomes a possibility.

Introducing  $z = (1 - 4gy) / (4g)^{2/3}$ , we re-express the differential equation as  $\Delta'' = z\Delta$ , whose solution is a linear combination of the Airy functions  $\text{Ai}(z)$  and  $\text{Bi}(z)$ . In terms of the original variable  $y$ ,

$$\Delta(y) = \Delta_0 \left( \text{Ai} \left( \frac{1 - 4gy}{(4g)^{2/3}} \right) + c \text{Bi} \left( \frac{1 - 4gy}{(4g)^{2/3}} \right) \right). \quad (43)$$

At  $y = 0$  and small  $g \ll 1$  the argument of the Airy functions is large and positive. Using the asymptotic expressions of  $\text{Ai}$  and  $\text{Bi}$ , we find from the boundary condition at  $y = 0$  that  $c \approx (g/4)e^{-\frac{1}{3g}}$  is exponentially small. Since both functions are comparable in magnitude at the UV boundary condition at  $y = Y$ , we can safely neglect  $\text{Bi}$  in (43), i.e., approximate the gap function by

$$\Delta(y) = \Delta_0 \text{Ai} \left( \frac{1 - 4gy}{(4g)^{2/3}} \right). \quad (44)$$

The UV boundary condition at  $y = Y$  then yields

$$\text{Ai} \left( \frac{1 - 4gY}{(4g)^{2/3}} \right) = (4g)^{1/3} \text{Ai}' \left( \frac{1 - 4gY}{(4g)^{2/3}} \right). \quad (45)$$

This condition determines the critical temperature through the  $T$ -dependence of  $Y(T_c) = \log(\Lambda^2/(mT_c))$ . For small  $g$ , the solutions of  $\text{Ai}(z) = (4g)^{1/3} \text{Ai}'(z)$  are  $z \approx z_n$ , where  $z_n$  is the  $n$ -th zero of the Airy function. The largest  $T_c$  corresponds to the first zero at  $z_0 \approx -2.338$ . For a more accurate analysis we expand Eq. (45) around  $z = z_0$  as  $\text{Ai}(z) \approx \text{Ai}'(z_0)(z - z_0)$  and  $\text{Ai}'(z) \approx \text{Ai}'(z_0) + \mathcal{O}((z - z_0)^2)$ . We then obtain  $1 - 4gY - z_0(4g)^{2/3} = 4g$  that yields

$$T_c = T_0 \exp \left( -\frac{1 + |z_0|(4g)^{2/3} - 4g}{4g} \right). \quad (46)$$

We plot this  $T_c$  in Fig. 4, where we also compare it with the full numerical solution of the gap equation (37) without self energy corrections (dashed and solid green lines, respectively). We verified that the numerical solution without the self-energy does reproduce the  $g^{2/3}$  dependence in the exponent for  $T_c$ , as in Eq. (46). Further comparing this equation with Eq. (36) we see that the leading exponential dependence in both formulas is the same  $e^{-1/(4g)}$ , i.e.  $\gamma = 4$ , larger in the numerics, but the additional  $O(g^{2/3})$  term in the numerator in Eq. (46) effectively reduces  $\gamma$ . We show in the next subsection that the self-energy corrections change the functional form of this term from  $O(g^{2/3})$  to  $O(1)$  such that the value of  $\gamma$  indeed gets reduced, in agreement with the numerical solution of the full gap equation.

The analytical  $\Delta(k_+)$  from Eq. (44) can be re-expressed as

$$\Delta(k_+) = \Delta_0 \text{Ai} \left( z_0 + (4g)^{1/3} \left( 1 - \log \frac{k_+}{\Lambda} \right) \right). \quad (47)$$

We remind that this formula is valid for  $k_+ > 2mT_c/\Lambda$ , where our computational procedure holds. At smaller  $k_+$ , we expect  $\Delta(k_+)$  to scale linearly with  $k_+$ . The gap function in Eq. (47) has a sharp maximum at

$$k_{\max} = \Lambda \exp \left( -\frac{|z_0| - |\tilde{z}_0| - (4g)^{1/3}}{(4g)^{1/3}} \right), \quad (48)$$

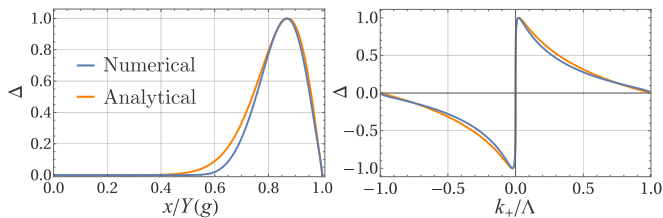


Figure 6. Momentum dependence of the triplet gap function for the ordinary VH point, obtained by solving the gap equation without self-energy corrections in the density of states kernel  $K(\bar{p})$ . The gap function is normalized to its maximal value. The two plots are on a logarithmic scale with  $x = \log\left(\frac{\Lambda k_+}{2mT}\right)$  (left panel) and on a linear scale (right panel). The dimensionless coupling constant is  $g = 0.01$ . The blue line is obtained by solving Eq. (37) numerically, and the orange line is the solution of Eq. (43). Notice that the region where the gap function is linear in momentum is narrower than in Fig. 5, which includes self-energy corrections.

where  $\tilde{z}_0 = -1.019$  ( $\text{Ai}'(\tilde{z}_0) = 0$ ). In Fig. 6 we compare  $\Delta(k_+)$  from (47) with the numerical solution of the original, integral gap equation without self-energy corrections. The agreement is quite good.

### 3. Analytic solution with self-energy included

In the two previous subsections we expanded the density of states  $K(p_+)$  of Eq. (21) to first order in  $g$  and, in doing so, neglected the fermionic self-energy. Such an expansion, however, holds only for  $p_+$  very near  $\Lambda$  and becomes problematic for somewhat smaller  $p_+$ , even if comparable to  $\Lambda$ . Indeed, in logarithmic variables the density of states is expressed as

$$K(y) = \frac{\log(1 + 2\log(2)gy(Y-y))}{\alpha g(Y-y)}. \quad (49)$$

Because typical  $y$  are comparable to  $Y$  and  $gY = O(1)$ , the expansion holds only when  $Y-y < 1$ . In the previous section, we expanded (49) to order  $g$ , but assumed that the solution of the differential equation holds even when  $Y-y \geq 1$ . Now we go beyond the linear order in  $g$  and demonstrate that this affects the results and improves the agreement with the numerical finding. We will not attempt to solve the gap equation with the full  $K(y)$  but rather expand it to second order in  $g$  and analyze how it affects  $T_c$ .

Expanding to order  $g^2$  and keeping in mind that the relevant  $y$  are still close to  $Y$ , we obtain

$$K(y) \approx y - gY^2(Y-y)\log 2. \quad (50)$$

Following the same computational steps as in the previous subsection, we obtain the differential gap equation

$$\Delta''(y) = V_{\text{eff}}(y)\Delta(y), \quad (51)$$

with effective potential

$$V_{\text{eff}}(y) = 1 - 4gK(y) = 1 - 4g_y(y - y_r) \quad (52)$$

where

$$g_y = g + (gY)^2 \log 2 \quad (53)$$

and

$$y_r = Y \frac{(gY)^2 \log 2}{g + (gY)^2 \log 2} \quad (54)$$

Introducing  $z = y - y_r$ , we re-express the differential gap equation as

$$\Delta''(z) = V_{\text{eff}}(z)\Delta(z), \quad (55)$$

where

$$V_{\text{eff}}(z) = 1 - 4g_y(z). \quad (56)$$

This equation is valid for  $y < Y$ , i.e., for  $z < Y_r$ , where

$$Y_r = Y - y_r = \frac{Y}{1 + gY^2 \log 2}. \quad (57)$$

This is the same equation as in the previous subsection, but with  $g_r$  instead of  $g$  and  $Y_r$  instead of  $Y$ . Accordingly, the expression for  $T_c$  is

$$Y_r = \frac{1 + |z_0|(4g_r)^{2/3} - 4g_r}{4g_r}. \quad (58)$$

Using  $Y_r = Yg/g_r$ , we re-express this relation as

$$Y = \frac{1 + |z_0|(4g_r)^{2/3} - 4g_r}{4g}. \quad (59)$$

Our previous result, Eq. (46), for  $T_c$  is reproduced if we set  $g_r = g$ , i.e. neglect the term with the prefactor  $\log 2$  in (53). We see, however, that the  $(gY)^2 \log 2$  term is *parametrically* larger than  $g$ , and hence  $g_r$  is larger than  $g$ . Substituting the expression for  $g_r$  into (59) and keeping only the leading term in  $g_r$ , we obtain the equation for  $a = gY$  in the form

$$4a = 1 + |z_0|(4\log 2)^{2/3}a^{2/3} - 4a\log 2. \quad (60)$$

The solution of this equation is  $a \approx 1/1.7544$ , i.e.,  $T_c \sim T_0 e^{-1/\gamma_r g}$  with  $\gamma_r = 1.7544$ . Expanding in Eq. (58) further to order  $g$  we obtain

$$T_c = T_0 e^{\frac{1+\mu_r g}{\gamma_r g}}, \quad (61)$$

with  $\mu_r = 2.092$ . The functional form of (61) is the same as extracted from the numerical solution of the gap equation, and the values of  $\gamma_r$  and  $\mu_r$  are reasonably close to numerical values in Eq. (25). To achieve a better agreement one would have to expand further in  $g$ . Still, the expansion of  $K(y)$  to order  $g^2$  clearly shows that the effect of keeping the self-energy is effectively a replacement of the  $g^{2/3}$  term in the numerator in the expression for  $T_c$  in (46) by a term of order one.

#### 4. Comparison with Son's model

It is also instructive to compare our result for  $T_c$  with the one for fermions away from VH singularity, but with an attractive logarithmic interaction. Such a model was originally solved by Son in the frequency domain[39], see also Ref. [40]. In momentum space, the corresponding gap equation in our notations  $\bar{k} = k/\Lambda$  has the form

$$\Delta(\bar{k}) = \frac{g}{2} \int_1^{\bar{\Lambda}} \frac{d\bar{p}}{\bar{p}} \log \frac{\bar{\Lambda}^2}{|\bar{k}^2 - \bar{p}^2|} \Delta(\bar{p}). \quad (62)$$

where  $\bar{\Lambda} = \Lambda^2/(2mT)$ , as before. We also keep the notation  $g$  for the dimensionless coupling constant. At a first glance, the effect of logarithmic interaction is the same as from logarithmic density of states at the VH point (Eqn. (22)). We show, however, that these two problems are rather distinct, because in our case the effective interaction  $\log \left| \frac{\bar{k} + \bar{p}}{\bar{k} - \bar{p}} \right|$ , while generally of order  $O(1)$ , is strongly reduced when one momenta is much smaller than the other one. This effectively eliminates the Cooper logarithm that emerges through  $d\bar{p}/\bar{p}$  in both (22) and (62). To demonstrate the distinct behavior of these two problems, we split the integral over  $\bar{p}$  in the r.h.s of (62) into regions  $\bar{p} < \bar{k}$  and  $\bar{p} > \bar{k}$ , as we did before, introduce logarithmic variables  $x = \log \bar{k}$ ,  $y = \log \bar{p}$  as well as  $Y = \log \bar{\Lambda}$ , and convert (62) into the the differential equation

$$\Delta''(x) = -g\Delta(x) \quad (63)$$

with boundary conditions

$$\begin{aligned} \Delta'(0) &= 0, \\ \Delta(Y) &= 0. \end{aligned} \quad (64)$$

The solution in terms of the original variable  $\bar{k}$  is

$$\Delta(\bar{k}) = \cos(\sqrt{g} \log \bar{k} + \phi). \quad (65)$$

We see that  $\Delta(\bar{k})$  oscillates as a function of  $\log \bar{k}$  for any value of  $g$ , even infinitesimally small ones. This is in contrast to our earlier discussion, where an oscillating solution holds only for  $\lambda$  above the threshold. The IR boundary condition yields  $\phi = l\pi$ , with integer  $l$ , while the UV condition yields  $\cos(\sqrt{g}Y) = 0$ , i.e.  $\sqrt{g}Y = (2l+1)\frac{\pi}{2}$ . The solution with  $l = 0$  gives the highest transition temperature

$$T_c = \frac{\Lambda_0^2}{2m} e^{-\frac{\pi}{2\sqrt{g}}}. \quad (66)$$

Other solutions with  $l > 0$  yield smaller  $T_c^{(l)} = \frac{\Lambda_0^2}{2m} e^{-\frac{(2l+1)\pi}{2\sqrt{g}}}$ . Comparing (66) to Eq. (1), we find that  $T_c$  for the single VH point is smaller as it contains  $1/g$  in the exponent as opposed to  $1/\sqrt{g}$  in Eq. (66). The distinction is due to the form of the pairing interaction in the triplet channel. In the case of pairing at the VH

point, the pairing strength alone is too weak to give rise to a Cooper instability. However, the enhanced phase space for scattering, which is a consequence of the logarithmic density of states, compensates for the weak interaction and yields, in the end, a BCS-type expression of the transition temperature.

#### B. Pairing at the extended VH point

Next we analyze extended VH points with a dispersion relation given in Eq. (5) for small but finite power-law exponent  $\epsilon$  that determines the density of states. We show in Appendix B that the inverse quasi-particle weight in this case is given by

$$Z_{\mathbf{k}} = \frac{2 \log 2}{4\epsilon^2} g \left( \left( \frac{\Lambda}{k_+} \right)^{2\epsilon} - 1 \right) \left( \left( \frac{\Lambda}{k_-} \right)^{2\epsilon} - 1 \right), \quad (67)$$

where the dimensionless coupling constant is now

$$g = \frac{U^2 \Lambda^{-4\epsilon}}{(4\pi^2 A)^2}. \quad (68)$$

Note that this  $g$  explicitly depends on the cutoff  $\Lambda$ . This will play a role when we consider the limit where  $g \ll \epsilon$ .

The gap equation can be written as

$$\begin{aligned} \Delta(k_+) &= -\frac{U^2 \Lambda^{-4\epsilon}}{4\pi A p_+^{1-2\epsilon}} \int_{p_0}^{\Lambda} \frac{dp_+}{\pi} K(p_+) \Delta_i(p_+) \\ &\times (\Pi(k_+ + p_+) - \Pi(k_+ - p_+)) \end{aligned} \quad (69)$$

where we introduced

$$K(p_+) = \frac{4\pi A p_+^{1-2\epsilon}}{\Lambda^{-4\epsilon}} \int_{-\Lambda}^{\Lambda} \frac{dp_-}{2\pi} \frac{\tanh\left(\frac{\epsilon p_-}{2(1+Z_p)T}\right)}{2\epsilon p_- (1+Z_p)}. \quad (70)$$

Here,  $p_0 = \frac{T}{A\Lambda^{1+2\epsilon}}$  is the temperature-dependent lower cutoff of the theory.

For the particle-particle bubble at small  $\epsilon$  we find

$$\Pi(k_+) = \frac{|k_+|^{-2\epsilon}}{8\pi^2 A \epsilon}. \quad (71)$$

This allows us to approximate the pairing kernel as

$$\Pi(k_+ + p_+) - \Pi(k_+ - p_+) = \begin{cases} 2\Pi'(k_+) p_+ & \text{if } p_+ \ll k_+ \\ 2\Pi'(p_+) k_+ & \text{if } k_+ \ll p_+ \end{cases} \quad (72)$$

with  $\Pi'(k_+) = -\frac{1}{4\pi^2 A} |k_+|^{-(1+2\epsilon)}$ .

Re-expressing the coupling in (69) in terms of the dimensionless  $g$  from (68), splitting the integration over  $p_+$  in into the ranges  $p_+ < k_+$  and  $p_+ > k_+$  and using Eq. (72), we re-express the gap equation as

$$\begin{aligned} \Delta(k_+) &= 2g \int_{k_0}^{k_+} dp_+ \frac{p_+^{2\epsilon}}{k_+^{1+2\epsilon}} K(p_+) \Delta_i(p_+) \\ &+ 2g \int_{k_+}^{\Lambda} dp_+ \frac{k_+}{p_+^2} K(p_+) \Delta_i(p_+). \end{aligned} \quad (73)$$

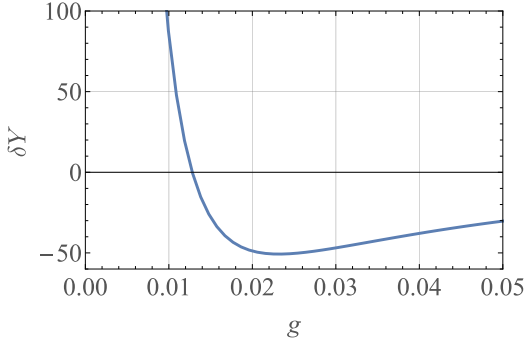


Figure 7. The dependence of  $\delta Y$  from Eq. (78) on the dimensionless coupling  $g$ , obtained from the numerical solution of the gap equation at an extended VH point, expanded to first order in  $\epsilon$ . The sign of  $\delta Y$  determines whether  $T_c$  for an extended VH point increases or decreases with  $\epsilon$ . For a negative  $\delta Y$ ,  $T_c$  increases, for a positive  $\delta Y$  it decreases. We see that  $\delta Y$  is positive at very small  $g$  and negative at larger  $g$ . The sign change occurs at  $g^* \approx 0.013$ . For small  $g$ ,  $\delta Y$  scales as  $1/g^2$ .

Rescaling the gap function as

$$\Delta(k_+) = \bar{\Delta} \left( \log \frac{k_+}{p_0} \right) \left( \frac{k_+}{\Lambda} \right)^{-\epsilon}$$

and introducing again the logarithmic variable

$$x = \log \frac{k_+}{p_0}, \quad (74)$$

we obtain a Schrödinger-type differential equation

$$-\frac{d^2 \bar{\Delta}}{dx^2} + V(x) \bar{\Delta} = 0, \quad (75)$$

with potential

$$V(x) = (1 + \epsilon)(1 + \epsilon - 4gK(p_0 e^x)). \quad (76)$$

The boundary conditions are now given as

$$\begin{aligned} \bar{\Delta}'(0) &= (1 + \epsilon) \bar{\Delta}(0), \\ \bar{\Delta}'(Y) &= -(1 + \epsilon) \bar{\Delta}(Y), \end{aligned} \quad (77)$$

where  $Y = \log \frac{\Lambda}{p_0} = \log \frac{A\Lambda^{2\epsilon}}{T}$  and  $T = T_c(\epsilon)$ . Below, we solve the gap equations in the limits where the ratio of the small dimensionless constants  $g$  and  $\epsilon$  is either large or small. In each case we compare the analytical results with the numerical solution of the gap equation.

### 1. The limit $\epsilon \ll g$

In this limit, we compute the leading correction in  $\epsilon/g$  to the expression for  $T_c$  for an ordinary VH point from first order perturbation theory for the Schrödinger equation, expanding the equation, the boundary condition,

and the potential  $V(x)$  to linear order in  $\epsilon$ . The resulting set of equations is then solved numerically and determines the correction  $\delta Y$  defined as

$$Y(\epsilon) = Y(\epsilon = 0) + \epsilon \delta Y. \quad (78)$$

The result for  $\delta Y$  is shown in Fig. 7. When  $g$  is larger than  $g^* \approx 0.013$ ,  $\delta Y$  is negative, hence the superconducting transition temperature increases with  $\epsilon$ . At smaller  $g < g^*$ ,  $\delta Y > 0$  and scales with  $g$  as  $1/g^2$ . The superconducting transition temperature decreases with  $\epsilon$  as

$$T_c(\epsilon) = T_c(\epsilon = 0) e^{-a\epsilon/g^2} \quad (79)$$

where  $a = O(1)$ . We emphasize that this  $T_c(\epsilon)$  smoothly connects to  $T_c(\epsilon = 0)$  at the ordinary VH point.

### 2. The limit $\epsilon \gg g$

We now show how the result for  $T_c$  gets modified in the opposite limit  $\epsilon \gg g$ . We set  $\epsilon$  to be a number of order one and compute  $T_c$  by order of magnitude, keeping the explicit dependence on  $\epsilon$  in the exponent, but neglecting the dependence on  $\epsilon$  in the prefactor. For  $\epsilon \gg g$ , we can safely take the limit  $\Lambda \rightarrow \infty$  as all integrals are UV convergent. Evaluating the integral for  $K(p_+)$  in (70) in infinite limits, we obtain

$$\begin{aligned} \lambda_\epsilon &\equiv 2gK(p_+) \\ &= \frac{4\epsilon^2}{\log 2} \int_{x_{\min}}^{\infty} \frac{dx}{|1+x|^{2(1+\epsilon)} - |1-x|^{2(1+\epsilon)}}, \end{aligned} \quad (80)$$

where  $x = p_-/p_+$  and  $x_{\min} \sim T/T_\epsilon$ , where  $T_\epsilon = A(p_+)^{2(1+\epsilon)}$ . Next, we assumed and verified that the relevant  $p_+$  in the equation for the pairing vertex are of order  $\Lambda g^{1/(4\epsilon)}$ . This allows us to express  $T_\epsilon \sim A\Lambda^{2(1+\epsilon)} g^{(1+\epsilon)/(2\epsilon)}$ .

The integral over  $x$  in (80) converges in the UV limit, which allows us to set the upper limit of the integration over  $x$  to infinity. It is logarithmically singular in the IR limit and with logarithmic accuracy we obtain  $\lambda_\epsilon \sim \log T_\epsilon/T = \log T_\epsilon/T_c(\epsilon)$ . Returning to the gap equation (75), we now have  $V(x) \approx (1 + \epsilon)(1 + \epsilon - 2\lambda_\epsilon) = \beta_\epsilon^2$ . The solution of Eq. (75) with such  $V$  is  $\bar{\Delta}(x) \sim e^{\pm\beta_\epsilon x}$ .

A similar power-law solution (as a function of frequency) holds for a number of quantum-critical systems [41] and Yukawa SYK-type models [42–44]. We verified that, like there, the solution, that satisfies boundary conditions, does not exist when  $\beta_\epsilon$  is real, but emerges when  $\beta_\epsilon$  becomes complex, and the onset of complex  $\beta_\epsilon$  sets the value of  $T_c$ . In our case,  $\beta_\epsilon$  becomes complex at  $\lambda_\epsilon = (1 + \epsilon)/2$ , which for a generic  $\epsilon$  is a number of order one. Using  $\lambda_\epsilon \sim \log T_\epsilon/T_c(\epsilon)$ , we then find that

$$T_c(\epsilon) \sim T_c \sim T_0 g^{(1+\epsilon)/(2\epsilon)}, \quad (81)$$

where  $T_0 \sim A\Lambda^{2(1+\epsilon)}$ . We see that  $T_c(\epsilon)$  is not exponentially small in  $g$ . We also notice that Eq. (81) can be

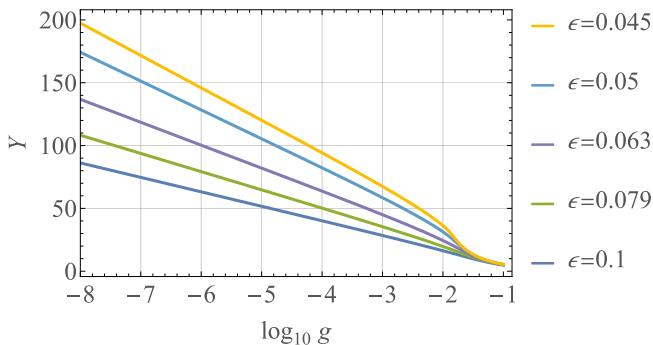


Figure 8. Dependence of  $Y(g, \epsilon) = \log \frac{T_0}{T_c(\epsilon)}$  on the coupling constant  $g$ , obtained by solving the gap equation numerically (see Sec. IV B 3). For  $\epsilon > g$  we find power-law behavior  $T_c \propto g^\alpha$ . The exponent  $\alpha$  is determined from the slope of  $Y(g, \epsilon)$  vs  $\log g$  and with high accuracy is  $\alpha \approx \frac{1}{2\epsilon}$ , consistent with our analytical analysis. For  $\epsilon < g$  the behavior deviates from the power-law dependence.

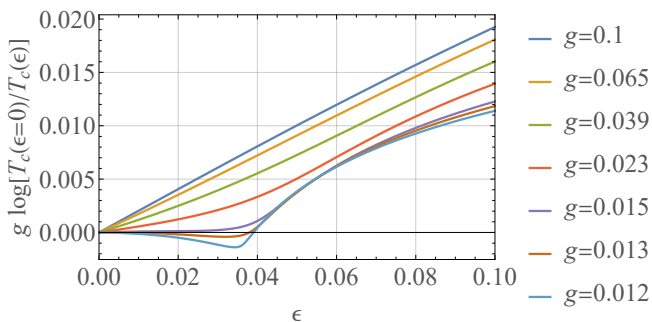


Figure 9. Dependence of  $g \log [T_c(\epsilon = 0)/T_c(\epsilon)]$  on  $\epsilon$  for different values of  $g$ , obtained by solving the gap equation numerically (see Sec. IV B 3). For  $g < g^* = 0.013$ , the dependence is non-monotonic, consistent with our analytical results. For larger  $g$ ,  $T_c(\epsilon)$  monotonically increases with  $\epsilon$ .

re-expressed, using (68), as

$$T_c(\epsilon) \sim A^{-1/\epsilon} U^{\frac{1+\epsilon}{\epsilon}}. \quad (82)$$

This last expression shows that  $T_c(\epsilon)$  does not depend on the upper cutoff  $\Lambda$  (the  $\Lambda$ -dependencies in  $T_0$  and  $g$  cancel out) and in this respect is universal.

At a qualitative level, we found that the crossover from  $T_c$  for an ordinary VH point to the one for an extended VH point is captured by the interpolation formula

$$\frac{1+\epsilon}{2\epsilon} \left( \left( \frac{T_0}{T_c(\epsilon)} \right)^{\frac{2\epsilon}{1+\epsilon}} - 1 \right) = \frac{1}{\gamma g}. \quad (83)$$

In the limit  $\epsilon \ll g$ , this reduces to  $\log T_0/T_c(\epsilon \rightarrow 0) = 1/\gamma g$ , in the opposite limit  $\epsilon \gg g$ , one recovers the universal power-law expression  $T_c(\epsilon) \sim T_0 g^{(1+\epsilon)/(2\epsilon)}$ .

### 3. Numerical solution for extended saddle points

We also performed the integration over the transverse momenta in the function  $K(p_+)$  in (70) numerically and solved numerically the gap equation (69) with this  $K(p_+)$ . We show the results in Figs. 8 and 9. In Fig. 8 we show the dependence of  $Y(g, \epsilon) = \log \left( \frac{T_0}{T_c(\epsilon)} \right)$  on the coupling constant  $g$ . The distinct behavior for  $\epsilon$  smaller and larger  $g$  is clearly visible. For  $\epsilon > g$  the linear dependence of  $Y$  on  $\log g$  demonstrates that the transition temperature  $T_c(\epsilon)$  has the power law form  $T_c(\epsilon) \propto g^\alpha$ . The value of  $\alpha$  is determined from the slope. The data are best described by  $T_c(\epsilon) \propto g^{\frac{1}{2\epsilon}}$ , consistent with (81). For  $\epsilon < g$  the behavior deviates from the power law. In Fig. 9 we show how the small  $\epsilon$  behavior of  $T_c(\epsilon)$  from Fig. 7 interpolates to the power-law behavior at larger  $\epsilon$ . For  $g < g^* = 0.013$ , the dependence of  $T_c(\epsilon)$  on  $\epsilon$  is non-monotonic, in agreement with our analytic findings.

## V. PAIRING FLUCTUATIONS, BKT TRANSITION AND CHARGE-4e SUPERCONDUCTIVITY

We next discuss the statistical mechanics that we expect to emerge from our analysis.

The solutions discussed in the previous section formally belong to a two-dimensional irreducible representation  $(\Delta(k_+), \Delta(k_-))$  of the point group. Hence, fluctuations of the order parameter might give rise to vestigial order with symmetry breaking of composite order parameters like nematic or time-reversal symmetry breaking states[47]. This is a consequence of the four-fold symmetric dispersions of Eqs. (4) and (5). However, the symmetry of a single VH point is usually lower and Eqs. (4) and (5) are the result of an anisotropic rescaling of momenta. This will lift the degeneracy of the two solutions and the triplet order parameter belongs to a one-dimensional representation of the point group.

For a 2D system one usually expects a Berezinskii–Kosterlitz–Thouless (BKT) transition[50, 51] to a state with algebraic order and with finite superfluid stiffness. As discussed by Halperin and Nelson[55], the resulting BKT transition temperature is very close to the mean field transition temperature that one obtains from the solution of the gap equation. The reason is that the threshold stiffness of the BKT transition is much smaller than the low- $T$  stiffness of a weakly coupled superconductor. Hence vortex proliferation sets in only very near the mean field transition temperature. However, the BKT physics does not hold for a triplet superconductor without spin-orbit interaction. Fluctuations of such a state are governed by the three-component complex coordinate-dependent field  $\psi(x) = (\psi_1(x), \psi_2(x), \psi_3(x))^T$  that describes long-wavelength variations of the pairing wave

function

$$\Psi_{\alpha\beta}(\mathbf{k}, \mathbf{x}) = \sum_{i=1}^3 \psi_i(\mathbf{x}) \Delta_i(\mathbf{k}) (\sigma^i i \sigma^y)_{\alpha\beta} \quad (84)$$

where  $\Delta_i(\mathbf{k})$  is the gap function discussed in the previous section. Fluctuations between components of  $\psi$ , i.e. fluctuations in the spin sector of the triplet state, destroy even an algebraic order due to the Hohenberg–Mermin–Wagner theorem[48, 49]. In the notation  $\psi = \psi_0 \mathbf{n} e^{i\theta}$  where  $\theta$  is the  $U(1)$  phase of the superconductor while the unit vector  $\mathbf{n}$  describes spin fluctuations of the triplet state, algebraic order of  $\psi$  is suppressed by fluctuations of  $\mathbf{n}$ .

The situation is different for a composite order parameter

$$\phi(\mathbf{x}) = \psi(\mathbf{x}) \cdot \psi(\mathbf{x}), \quad (85)$$

which describes a charge- $4e$  superconductor, in which two triplets form a singlet in spin space[52, 53]. Since  $\mathbf{n}^2 = 1$  it follows that

$$\langle \phi^*(x) \phi(x') \rangle = \psi_0^4 \left\langle e^{-2i(\theta(x) - \theta(x'))} \right\rangle, \quad (86)$$

i.e.,  $\phi$  possesses only phase fluctuations, which allow a BKT transition. The extra factor 2 in the exponent in (86) allows for fractionalized vortices of the primary superconducting order parameter (the spin field heals the mismatch that forms at a fractional vortex, see Ref. [58]). The threshold stiffness for the BKT transition in a charge- $4e$  superconductor is four times larger than that for a charge- $2e$  superconductor, yet it is still much smaller than the zero temperature stiffness. Hence, the  $4e$  BKT transition still occurs very near mean-field  $T_c$  for the primary  $2e$  order parameter. If spin-orbit interaction is present, the anisotropy in spin space suppresses fluctuations and allows charge- $2e$  superconductivity with an algebraic order.

## VI. SUMMARY

In this work we analyzed low-temperature instabilities of a system of fermions with a single ordinary or extended VH point at the Fermi level, in the limit of small electron-electron interactions.

We first considered the possibility of ferromagnetic order and argued that it likely does not develop because of strong reduction of particle-hole response in the  $\mathbf{q} \rightarrow \mathbf{0}$  limit by particle-particle fluctuations.

We then analyzed pairing instabilities and explicitly demonstrated both, analytically and numerically, that a system with a single VH point at the Fermi level is unstable towards triplet superconductivity. The instability develops for both a conventional and a higher-order VH point, but  $T_c$  is much higher for a higher-order VH point in the regime  $\epsilon > g$ , where it varies with the coupling constant  $g$  in a power-law fashion, as  $T_c \propto g^{(1+\epsilon)/(2\epsilon)}$ .

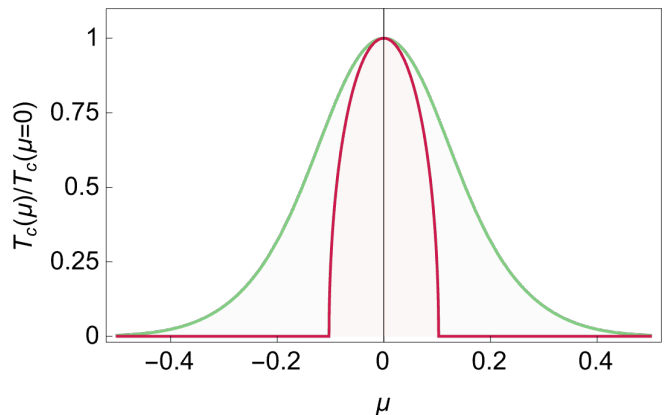


Figure 10. A schematic plot of the dependence of  $T_c$  on detuning from the VH point by a parameter  $\mu$  (e.g. a non-zero chemical potential) In our case (red curve), the transition temperature, determined by Eq. (88), vanishes when detuning exceeds  $T_c(\mu = 0)$ . In the case of a constant attraction (green curve), the transition temperature, determined by Eq. (87), gets reduced upon detuning from the VH point, but remains finite.

We showed that this  $T_c$  is a universal, cutoff independent quantity, determined by the band curvature and the local interaction.

The attractive triplet component of the pairing vertex comes from the Kohn-Luttinger type dressing of the pairing interaction by particle-hole fluctuations. Yet, we demonstrated that the mechanism for superconductivity is distinct from the usual Kohn-Luttinger one. In our problem, the attractive component of the vertex function is weak and, on its own, would not lead to a Cooper instability. However, the enhancement of the density of states near a VH point overcomes the smallness of the pairing vertex and gives rise to a BCS-like expression for  $T_c$  for an ordinary VH point and to power-law dependence of  $T_c$  on the coupling for an extended VH point.

As a consequence of this fundamentally non-BCS pairing mechanism, the transition temperature is expected to rapidly drop once the system moves away from a VH singularity under, e.g., a change of the chemical potential. Given the absence of a Cooper phenomenon, we expect that away from a VH singularity, superconductivity will develop only if the coupling exceeds a certain threshold. For any given  $g$ , there will be then a superconducting quantum critical point at some detuning. Similar behavior occurs for pairing at a critical point towards density-wave order and in SYK models [41–45].

To illustrate this effect we compare  $T_c(\mu)$  for our system and for a system with a constant attraction  $g$  and a logarithmic density of states, detuned by  $\mu$  (a detuned version of the model discussed by Son, see IV A 4). In the last case, the transition temperature is determined by

$$1 = \frac{4}{\pi^2} g \log \left( \frac{T_0}{T_c} \right) \log \left( \frac{T_0}{\sqrt{T_c^2 + \mu^2}} \right), \quad (87)$$

where  $T_c(\mu = 0) \propto e^{-\pi/(2\sqrt{g})}$ , see Eq. (66). For  $|\mu| > T_c(\mu = 0)$ , the effective coupling constant is reduced, yet  $T_c(\mu)$  remains finite. For our problem,  $T_c(\mu)$  is determined by

$$1 = \gamma g \log \left( \frac{T_0}{\sqrt{T_c^2 + \mu^2}} \right) \quad (88)$$

and remains non-zero only at  $|\mu| < T_c(\mu = 0)$ . For larger detuning from a VH point,  $T_c = 0$ . This sets a superconducting quantum critical point at  $|\mu| \sim T_c(\mu = 0)$ . We illustrate this in Fig. 10.

We also discussed the role of critical fluctuations and argued that the transition temperature that we derived from the linearized gap equation is close to a BKT transition into an algebraic superconductor, which in the absence of spin-orbit interaction is a charge- $4e$  superconductor made up of singlet bound states of triplet pairs, and in the presence of spin-orbit interaction is a charge- $2e$  superconductor.

In our analysis we concentrate on processes that are exclusively due to interactions between fermions at or

near a VH point. It is important to keep in mind that some crucial physical processes may come from electronic states away from a VH point, particularly for transport phenomena[21]. For thermodynamic instabilities, the instability that we found here is, however, the leading one in the pairing channel in the limit of weak coupling.

## ACKNOWLEDGMENTS

We are grateful to Erez Berg, Joseph Betouras, Anzumaan Chakraborty, Laura Classen, Elio König, Mohid Randeria, Michael Scherrer, and Veronika Stangier for helpful discussions. This work was supported by the German Research Foundation TRR 288-422213477 ELASTO-Q-MAT, Projects A11 (MG) and B01 (RO, JS), a Weston Visiting Professorship at the Weizmann Institute of Science (JS), and by National Science Foundation grant NSF: DMR - 2325357 (AVC and YCL). Part of the work was performed when JS and AVC visited KITP at UCSB. KITP is supported in part by the National Science Foundation under PHY-1748958.

- 
- [1] L. Van Hove, *The occurrence of singularities in the elastic frequency distribution of a crystal*, Phys. Rev. 89, 1189 (1953).
- [2] J. L. McChesney, A. Bostwick, T. Ohta, T. Seyller, K. Horn, J. González, and E. Rotenberg, *Extended Van Hove Singularity and Superconducting Instability in Doped Graphene*, Phys. Rev. Lett. 104, 136803 (2010).
- [3] R. Nandkishore, L. Levitov, and A. Chubukov, *Chiral superconductivity from repulsive interactions in doped graphene*, Nat. Phys. 8, 158 (2012).
- [4] M. L. Kiesel, C. Platt, W. Hanke, D. A. Abanin, and R. Thomale, *Competing many-body instabilities and unconventional superconductivity in graphene*, Phys. Rev. B 86, 020507(R) (2012).
- [5] W.-S. Wang, Y.-Y. Xiang, Q.-H. Wang, F. Wang, F. Yang, and D.-H. Lee, *Functional renormalization group and variational Monte Carlo studies of the electronic instabilities in graphene near 1/4 doping*, Phys. Rev. B 85, 035414 (2012).
- [6] A. M. Black-Schaffer and C. Honerkamp, *Chiral d-wave superconductivity in doped graphene*, J. Phys.: Condens. Matter 26, 423201 (2014).
- [7] A. Shtyk, G. Goldstein, and C. Chamon, *Electrons at the monkey saddle: A multicritical Lifshitz point*, Phys. Rev. B 95, 035137 (2017).
- [8] N. F. Yuan, H. Isobe, and L. Fu, *Magic of high-order Van Hove singularity*, Nat. Commun. 10, 1 (2019).
- [9] H. Isobe and L. Fu, *Supermetal*, Phys. Rev. Res. 1, 033206 (2019).
- [10] N. F. Q. Yuan and L. Fu, *Classification of critical points in energy bands based on topology, scaling, and symmetry*, Phys. Rev. B 101, 125120 (2020).
- [11] A. Chandrasekaran, A. Shtyk, J. J. Betouras, and C. Chamon, *Catastrophe theory classification of fermi surface topological transitions in two dimensions*, Phys. Rev. Res. 2, 013355 (2020).
- [12] L. Classen, A. V. Chubukov, C. Honerkamp, and M. M. Scherer, *Competing orders at higher-order Van Hove points*, Phys. Rev. B 102, 125141 (2020).
- [13] Jiawei Zang, Jie Wang, Jennife Cano and Andrew J. Millis, *Hartree-Fock study of the moiré Hubbard model for twisted bilayer transition metal dichalcogenides*, Phys. Rev. B. 104, 075150 (2021).
- [14] W.-S. Wang, Z.-Z. Li, Y.-Y. Xiang, and Q.-H. Wang, *Competing electronic orders on kagome lattices at van Hove filling*, Phys. Rev. B 87, 115135 (2013)
- [15] Y. Hu, X. Wu, B. R. Ortiz, S. Ju, X. Han, J. Ma, N. C. Plumb, M. Radovic, R. Thomale, S. D. Wilson, A. P. Schnyder, and M. Shi, *Rich nature of Van Hove singularities in Kagome superconductor CsV<sub>3</sub>Sb<sub>5</sub>*, Nature Comm. 13, 2220 (2022).
- [16] M. Kang, S. Fang, J.-K. Kim, B. R. Ortiz, S. H. Ryu, J. Kim, J. Yoo, G. Sangiovanni, D. Di Sante, B.-G. Park, C. Jozwiak, A. Bostwick, E. Rotenberg, E. Kaxiras, S. D. Wilson, J.-H. Park, and R. Comin, *Twofold van Hove singularity and origin of charge order in topological kagome superconductor CsV<sub>3</sub>Sb<sub>5</sub>*, Nat. Phys. 18, 301 (2022).
- [17] D. V. Efremov, A. Shtyk, A. W. Rost, C. Chamon, A. P. Mackenzie, and J. J. Betouras, *Multicritical Fermi Surface Topological Transitions*, Phys. Rev. Lett. 123, 207202 (2019).
- [18] C. W. Hicks, D. O. Brodsky, E. A. Yelland, A. S. Gibbs, J. A. N. Bruin, M. E. Barber, S. D. Edkins, K. Nishimura, S. Yonezawa, Y. Maeno, and A. P. Mackenzie, *Strong increase of T<sub>c</sub> of Sr<sub>2</sub>RuO<sub>4</sub> under both tensile and compressive strain*, Science 344, 283 (2014).
- [19] M. E. Barber, A. S. Gibbs, Y. Maeno, A. P. Mackenzie, and C. W. Hicks, *Resistivity in the Vicinity of a Van Hove Singularity: Sr<sub>2</sub>RuO<sub>4</sub> under Uniaxial Pressure*, Phys. Rev. Lett. 120, 076602 (2018).

- [20] Y.-S. Li, M. Garst, J. Schmalian, N. Kikugawa, D. A. Sokolov, C. W. Hicks, F. Jerzembeck, M. S. Ikeda, A. W. Rost, M. Nicklas, and A. P. Mackenzie, *Elastocaloric determination of the phase diagram of  $Sr_2RuO_4$* , Nature 607, 276 (2022).
- [21] V. C. Stangier, E. Berg, and J. Schmalian, *Breakdown of the Wiedemann-Franz law at the Lifshitz point of strained  $Sr_2RuO_4$* , Phys. Rev. B 105, 115113 (2022).
- [22] I. E. Dzyaloshinskii, *Superconducting transitions due to Van Hove singularities in the electron spectrum*, Zh. Eksp. Teor. Fiz. 93, 1487 (1987) [Sov. Phys. JETP 66, 848 (1987)].
- [23] I. E. Dzyaloshinskii and V. M. Yakovenko, *Weak coupling theory for  $La_2CuO_4$* , Zh. Eksp. Teor. Fiz. 94, 344 (1988) [Sov. Phys. JETP 67, 844 (1988)].
- [24] A. Virosztek and J. Ruvalds, *Nested-Fermi-liquid theory*, Phys. Rev. B 42, 4064 (1990).
- [25] D. M. Newns, C. C. Tsuei and P. C. Pattnaik, *Van Hove scenario for d-wave superconductivity in cuprates*, Phys. Rev. B 52, 13611 (1995).
- [26] R. Hlubina, *Effect of impurities on the transport properties in the Van Hove scenario*, Phys. Rev. B 53, 11344 (1996).
- [27] N. Furukawa, T. M. Rice, and M. Salmhofer, *Truncation of a Two-Dimensional Fermi Surface due to Quasiparticle Gap Formation at the Saddle Points*, Phys. Rev. Lett. 81, 3195 (1998).
- [28] J. V. Alvarez, J. Gonzalez, F. Guinea, and M. A. H. Vozmediano, *Superconducting, Ferromagnetic and Antiferromagnetic Phases in the  $tt'$  Hubbard Model*, J. Phys. Soc. Jpn. 67, 1868 (1998).
- [29] C. Honerkamp and M. Salmhofer, *Temperature-flow renormalization group and the competition between superconductivity and ferromagnetism*, Phys. Rev. B 64, 184516 (2001).
- [30] V. Yu. Irkhin, A. A. Katanin, and M. I. Katsnelson, *Effects of van Hove singularities on magnetism and superconductivity in the  $t-t'$  Hubbard model: A parquet approach*, Phys. Rev. B 64, 165107 (2001).
- [31] K. Le Hur and T. M. Rice, *Superconductivity close to the Mott state: From condensed-matter systems to superfluidity in optical lattices*, Ann. Phys. (NY) 324, 1452 (2009).
- [32] C. Husemann and M. Salmhofer, *Efficient parametrization of the vertex function, scheme, and the  $t,t'$  Hubbard model at van Hove filling*, Phys. Rev. B 79, 195125 (2009).
- [33] I. Dzyaloshinskii, *Extended Van-Hove singularity and related non-Fermi liquids*, Journal de Physique I 6.1, 119 (1996).
- [34] D. Menashe and B. Laikhtman, *Fermi-liquid properties of a two-dimensional electron system with the Fermi level near a van Hove singularity*, Phys. Rev. B 59, 13592 (1999).
- [35] W. Kohn and J. M. Luttinger, *New Mechanism for Superconductivity*, Phys. Rev. Lett. 15, 524 (1965).
- [36] A. V. Chubukov, *Kohn-Luttinger effect and the instability of a two-dimensional repulsive Fermi liquid at  $T = 0$* , Phys. Rev. B 48, 1097 (1993).
- [37] R. Shankar, *Renormalization-group approach to interacting fermions*, Rev. Mod. Phys. 66, 129 (1994).
- [38] D. P. Arovas, E. Berg, S. A. Kivelson, and S. Raghu, *The Hubbard Model*, Ann. Rev. of Cond. Mat. Phys. 13, 239, (2022).
- [39] D. T. Son, *Superconductivity by long-range color magnetic interaction in high-density quark matter*, Phys. Rev. D 59, 094019 (1999)
- [40] A. V. Chubukov and J. Schmalian, *Superconductivity due to massless boson exchange in the strong-coupling limit*, Phys. Rev. B 72, 174520 (2005)
- [41] Ar. Abanov and A. V. Chubukov *Interplay between superconductivity and non-Fermi liquid at a quantum-critical point in a metal. I: The  $\gamma$ -model and its phase diagram at  $T=0$ . The case  $0 < \gamma < 1$* , Phys. Rev. B 102, 024524 (2020).
- [42] I. Esterlis and J. Schmalian, *Cooper pairing of incoherent electrons: an electron-phonon version of the Sachdev-Ye-Kitaev model*, Phys. Rev. B 100, 115132 (2019).
- [43] Y. Wang *Solvable Strong-Coupling Quantum-Dot Model with a Non-Fermi-Liquid Pairing Transition*, Phys. Rev. Lett. 124, 017002 (2020).
- [44] L. Classen and A. V. Chubukov *Superconductivity of incoherent electrons in Yukawa-SYK model*, Phys. Rev. B 104, 125120 (2021).
- [45] A. V. Chubukov, A. Abanov, Y. Wang and Y-M Wu, *The interplay between superconductivity and non-Fermi liquid at a quantum-critical point in a metal*, Annals of Physics, 417, 168142, (2020).
- [46] A. A. Abrikosov; L. P. Gorkov; I. E. Dzyaloshinski, *Methods Of Quantum Field Theory In Statistical Physics*, Prentice-Hall Inc., Englewood Cliffs, New Jersey (1963).
- [47] R. M. Fernandes, P.P. Orth, and J. Schmalian, *Intertwined vestigial order in quantum materials: nematicity and beyond*, Annu. Rev. Condens. Matter Phys. 10, 133–154 (2019).
- [48] P. C. Hohenberg, *Existence of Long-Range Order in One and Two Dimensions*, Phys. Rev. 158, 383 (1967).
- [49] N. D. Mermin and H. Wagner, *Absence of Ferromagnetism or Antiferromagnetism in One- or Two-Dimensional Isotropic Heisenberg Models*, Phys. Rev. Lett. 17, 1133 (1966); Erratum Phys. Rev. Lett. 17, 1307 (1966).
- [50] J. M. Kosterlitz and D. J. Thouless, *Ordering, metastability and phase transitions in two-dimensional systems*, J. Phys. C 6, 1181 (1973).
- [51] J. M. Kosterlitz, *The critical properties of the two-dimensional XY model*, J. Phys. C 7, 1046 (1974).
- [52] S. E. Korshunov, *Two-dimensional superfluid Fermi liquid with p-wave pairing*, Sov. Phys. JETP 62, 301 (1985); Zh. Eksp. Teor. Fiz. 89, 531 (1985).
- [53] J. Schmalian, *Interface superconductivity*, in Handbook of Superconductivity; Fundamentals and Materials, Volume One; edited by David A. Cardwell, David C. Larbalestier, Aleksander Braginski Edition, 2nd Edition; Taylor and Francis (2021).
- [54] J. Pearl, *Current distribution in superconducting films carrying quantized fluxoids*, Appl. Phys. Lett. 5, 65 (1964).
- [55] B. I. Halperin and D. R. Nelson, *Resistive Transition in Superconducting Films*, Journal of Low Temp. Phys. 36, 599 (1979).
- [56] T.-L. Ho, *Spinor Bose Condensates in Optical Traps*, Phys. Rev. Lett. 81, 742 (1998).
- [57] A. J. A. James and A. Lamacraft, *Phase Diagram of Two-Dimensional Polar Condensates in a Magnetic Field*, Phys. Rev. Lett 106, 140402 (2001).
- [58] S. Mukerjee, C. Xu, and J. E. Moore, *Topological Defects and the Superfluid Transition of the  $s = 1$  Spinor Condensate in Two Dimensions*, Phys. Rev. Lett. 97,

120406 (2006).  
 [59] J. M. Fellows, S. T. Carr, C. A. Hooley, and J. Schmalian, *Unbinding of Giant Vortices in States of Competing Order*, Phys. Rev. Lett. **109**, 155703 (2012).

[60] S. Maiti and A. V. Chubukov, *Superconductivity from repulsive interaction*, in "Novel Superfluids", Bennemann, K. H. and Ketterson, John B. eds, Oxford University Press 2014.

## APPENDIX A. A POTENTIAL FERROMAGNETIC INSTABILITY

In this Appendix we present the details of our analysis of a potential instability towards ferromagnetism. For definiteness, we consider a single ordinary VH point with dispersion  $\epsilon_k = (k_x^2 - k_y^2)/(2m)$ . The Stoner instability can be detected by computing the static and uniform magnetic susceptibility  $\chi$  (the limit  $q \rightarrow 0$  of the static  $\chi(q)$ ). This susceptibility can be obtained by either introducing an infinitesimal magnetic field and computing magnetization or by introducing an infinitesimal bare ferromagnetic order parameter, dressing it by the interactions, and computing the ratio of the fully dressed and the bare order parameters. In the diagrammatic analysis, the second approach is easier to implement. The bare order parameter  $\Delta_0$  is represented as a two-particle vertex, and the dressed one  $\Delta$  is obtained by renormalizing this vertex by the interactions (see Fig. 2(c)). In the ladder approximation,  $\Delta = \Delta_0 (1 + U\Pi_{\text{ph}}(0,0) + (U\Pi_{\text{ph}}(0,0))^2 + \dots)$ , where  $\Pi_{\text{ph}}(0,0)$  is the static particle-hole bubble  $\Pi_{\text{ph}}(q, \Omega = 0)$  in the limit  $q = 0$ . The perturbative series are geometrical, and the susceptibility, defined as  $\chi = \Delta/\Delta_0$ , is

$$\chi = \frac{1}{1 - U\Pi_{\text{ph}}(0,0)}. \quad (\text{S1})$$

For an ordinary VH point,

$$\Pi_{\text{ph}}(0,0) = \frac{ml}{2\pi^2}, \quad (\text{S2})$$

where

$$l = \log \frac{\Lambda^2}{mT} \quad (\text{S3})$$

and  $\Lambda \sim p_F$  is the upper momentum cutoff. Within this approximation, a ferromagnetic instability develops at any  $U$ , at a temperature much larger than the superconducting  $T_c$ , which we obtained in the main text. If this was the case, our consideration of the pairing instability would be invalid.

The summation of the ladder series can be reformulated in the RG language as the solution of the differential RG equation for the running  $\Delta(l)$  in terms of the running static coupling  $\lambda_{\text{ph}}(l)$  at zero momentum transfer. The equations for running  $\Delta(l)$  and  $\lambda_{\text{ph}}(l)$  are

$$\frac{d\Delta(l)}{dl} = \lambda_{\text{ph}}(l)\Delta(l), \quad (\text{S4})$$

$$\frac{d\lambda_{\text{ph}}(l)}{dl} = (\lambda_{\text{ph}}(l))^2, \quad (\text{S5})$$

and the bare value of the coupling is

$$\lambda_{\text{ph}}(0) = \lambda_0 = \frac{mU}{2\pi^2}. \quad (\text{S6})$$

The solution of these equations is Eq. (S1) with  $U\Pi_{\text{ph}}(0,0) = \lambda_0 l$ , i.e.,

$$\chi = \frac{1}{1 - \lambda_0 l}. \quad (\text{S7})$$

As we said in the main text, the ladder approximation should not be trusted in our case because the two-particle vertex in Fig. 2 also get renormalizations from the particle-particle channel. The static and uniform  $\Pi_{\text{pp}}(0,0)$  scales as  $l^2$  due to the combination of the logarithmic singularity in the density of states and the Cooper logarithm:

$$\Pi_{\text{pp}}(0,0) = -\frac{m}{4\pi^2} l^2. \quad (\text{S8})$$

The polarization  $\Pi_{\text{pp}}(0, 0)$  renormalizes the static coupling  $\lambda_{\text{pp}}(l)$  with zero total incoming momentum. The ladder series of the renormalizations in the particle-particle channel yield

$$\lambda_{\text{pp}}(l) = \frac{\lambda_0}{1 + \lambda_0 l^2}. \quad (\text{S9})$$

Because  $\lambda_0 > 0$ , the running coupling in the particle-particle channel decreases as  $l$  increases. This behavior can again be reformulated in RG as the flow equation

$$\frac{d\lambda_{\text{pp}}(l)}{dl} = -2l (\lambda_{\text{pp}}(l))^2. \quad (\text{S10})$$

Beyond the ladder approximation, there are cross-renormalizations of  $\lambda_{\text{ph}}(l)$  in the particle-particle channel and of  $\lambda_{\text{pp}}(l)$  in the particle-hole channel. Within RG, it seems natural to add the two contributions to the RG flow of each coupling. For  $\lambda_{\text{ph}}(l)$ , this would mean that the RG equation becomes, instead of (S5),

$$\frac{d\lambda_{\text{ph}}(l)}{dl} = (\lambda_{\text{ph}}(l))^2 (1 - 2l). \quad (\text{S11})$$

Solving (S11) one would then obtain

$$\lambda_{\text{ph}}(l) = \frac{\lambda_0}{1 + \lambda_0 l (l - 1)} \quad (\text{S12})$$

and

$$\chi(l) = \exp \left[ \left( \frac{2\lambda_0}{4 - \lambda_0} \right)^{1/2} \left( \arctan(2l - 1) \left( \frac{\lambda_0}{4 - \lambda_0} \right)^{1/2} + \arctan \left( \frac{\lambda_0}{4 - \lambda_0} \right)^{1/2} \right) \right]. \quad (\text{S13})$$

This  $\chi(l)$  saturates at large  $l$  instead of diverging, hence within RG there is no ferromagnetic instability: renormalizations in the particle-hole channel, which increase the running coupling and would nominally lead to such an instability, are overshoot by stronger renormalizations in the particle-particle channel, which reduce the coupling.

This analysis, however, assumes that the renormalizations of the coupling in the two channels just add up. This needs to be verified because the  $l^2$  renormalization in the particle-particle channel holds for the interaction  $\lambda_{\text{pp}}$  with zero total momentum, while for the analysis of potential ferromagnetism we need to know  $\lambda_{\text{ph}}$  at zero momentum transfer. For this reason, below we explicitly compute the two-loop diagram for the renormalization of the vertex  $\Delta(l)$ , by combining the renormalizations in the particle-hole and particle-particle channels. We show the corresponding diagram in Fig. 2(c). The one-loop vertex renormalization holds in the particle-hole channels and yields the correction  $\lambda_0 l$ . If the RG treatment is correct, at least qualitatively, the mixed two-loop diagram must give  $O(l^3)$ . We show below that the  $l^3$  term vanishes and the actual dependence is  $l^2$ .

The calculation proceeds in a standard way. We set external momenta to values at the VH point and the external fermionic Matsubara frequency to  $\pi T$ , and use the temperature as IR cutoff. The quantity we need to calculate is

$$X = \int_p G^2(p - p_0) \Pi_{\text{pp}}(p), \quad (\text{S14})$$

where  $p = (\mathbf{p}, \Omega)$  and  $\Omega$  is Matsubara frequency, and  $p_0 = (0, \pi T)$ . We use momentum variables  $p_{+-} = (p_x \pm p_y)/\sqrt{2}$ . In these variables, the fermionic dispersion is  $\epsilon_{\mathbf{p}} = p_+ p_- / m$ .

The polarization bubble  $\Pi_{\text{pp}}(p)$  is the convolution of the Green's functions of two fermions with  $l = (\mathbf{l}, \omega)$  and  $l + p = (\mathbf{l} + \mathbf{p}, \omega + \Omega)$ . Summing over  $\omega$ , we obtain

$$\Pi_{\text{pp}}(p) = \int \int \frac{dl_+ dl_-}{4\pi^2} \frac{1 - n_F \left( \frac{l_+ l_-}{m} \right) - n_F \left( \frac{(l_+ + p_+)(l_- + p_-)}{m} \right)}{\epsilon_{l,p} - i\Omega} \quad (\text{S15})$$

where  $\epsilon_{l,p} = \frac{l_+ l_-}{m} + \frac{(l_+ + p_+)(l_- + p_-)}{m}$ . Combining this with  $G^2(p - p_0)$ , summing over  $\Omega$ , and neglecting  $\pi T$ , which is irrelevant to the analysis of the power of  $l$ , we obtain  $X = X_1 + X_2$ , where

$$X_1 = \int \int \frac{dl_+ dl_-}{4\pi^2} \int \int \frac{dp_+ dp_-}{4\pi^2} \left( 1 - n_F \left( \frac{l_+ l_-}{m} \right) - n_F \left( \frac{(l_+ + p_+)(l_- + p_-)}{m} \right) \right) \frac{n_F(\epsilon_{l,p}) - n_F(\epsilon_p)}{(\epsilon_p - \epsilon_{l,p})^2} \quad (\text{S16})$$

and

$$X_2 = \int \int \frac{dl_+ dl_-}{4\pi^2} \int \int \frac{dp_+ dp_-}{4\pi^2} \frac{1}{4T \cosh^2 \frac{\epsilon_p}{2T}} \frac{1 - n_F\left(\frac{l_+ l_-}{m}\right) - n_F\left(\frac{(l_+ + p_+)(l_- + p_-)}{m}\right)}{\epsilon_{l,p} - \epsilon_p}. \quad (\text{S17})$$

The upper limit of momentum integration is  $\Lambda$ , the lower limit is effectively set by  $(mT)^{1/2}$  because of Fermi functions. Each of the two terms gives  $O(l^3)$ . This can be seen most straightforwardly by evaluating  $X_2$ . Here, typical  $\epsilon_p$  are of order  $T$ . Re-expressing  $\int \int dp_+ dp_- / (4\pi^2)$  as  $(m/4\pi^2) \int dp_+ / p_+ \int d\epsilon_p$  and keeping typical  $l_+, l_-$ , and  $p_+$  much larger than  $T$  by absolute value, in anticipation of the logarithms, one can re-express  $X_2$  as

$$X_2 = \frac{m}{16\pi^4} \int \frac{dp_+}{|p_+|} \int \int dl_+ dl_- \frac{1 - n_F\left(\frac{l_+ l_-}{m}\right) - n_F\left(\frac{(l_+ + p_+)(l_- + p_-)}{m}\right)}{\epsilon_{l,p}} \times I \quad (\text{S18})$$

where the integral  $I$  simplifies due to

$$I = \frac{1}{4T} \int_{-\infty}^{\infty} \frac{d\epsilon_p}{\cosh^2 \frac{\epsilon_p}{2T}} = 1. \quad (\text{S19})$$

To estimate the  $l$ -dependence of  $X_2$ , we note that for  $l > p$  and  $\epsilon_l > mT$ , the numerator in (S18) is  $\text{sign}\epsilon_l$  and  $\epsilon_{l,p} \approx \epsilon_l = l_+ l_- / m$ . Rescaling then  $p_+, l_+$  and  $l_-$  by  $(mT)^{1/2}$ , converting the integration to positive variables, and using the squares of the original variables as the new ones, which we label  $a, b$  and  $c$ , we obtain

$$X_2 = \frac{m^2}{16\pi^4} \int_1^l \frac{da}{a} \int_1^l \frac{db}{b} \int_1^l \frac{dc}{c} = \frac{m^2}{16\pi^4} l^3. \quad (\text{S20})$$

A similar analysis can be done for  $X_1$ . Here we note that

$$\int d\epsilon_p \frac{n_F(\epsilon_{l,p}) - n_F(\epsilon_p)}{(\epsilon_p - \epsilon_{l,p})^2} \approx -\frac{1}{\epsilon_{l,p}} \quad (\text{S21})$$

and hence

$$X_1 = -\frac{m}{16\pi^4} \int \frac{dp_+}{|p_+|} \int \int dl_+ dl_- \frac{1 - n_F\left(\frac{l_+ l_-}{m}\right) - n_F\left(\frac{(l_+ + p_+)(l_- + p_-)}{m}\right)}{\epsilon_{l,p}} \times I. \quad (\text{S22})$$

Evaluating the remaining integral in the same way as we did for  $X_2$ , we find  $X_1 = -\frac{m^2}{16\pi^4} l^3$ . However, comparing (S22) and (S18), we see that they are exactly opposite to each other. This holds even before we approximate each term by (S20). As a result, the  $l^3$  terms in  $X_1$  and  $X_2$  cancel each other, even if we compute each with more care than we did in moving from (S18) to (S20). We emphasize that to detect the cancellation, one must keep frequency dependence in  $\Pi_{pp}(p)$ . If we approximated the particle-particle polarization by its static form  $\Pi_{pp}(\mathbf{p}, \Omega = 0)$ , we would get  $X = X_2$ , with no  $X_1$  term. In this situation, the  $l^3$  term in  $X$  would be present.

The next term in  $X$  is of order  $l^2$ , and there is no reason why such a term may cancel. We computed  $X$  numerically and did find that  $X$  scales as  $l^2$ . Explicitly, we found

$$X \approx -b (\lambda_0 l)^2, \quad (\text{S23})$$

where  $b \approx 1.8$ . To order  $\lambda_0^2$ , the renormalization in the particle-particle channel then changes the bare coupling to  $\lambda_{\text{eff}} = \lambda_0(1 - b\lambda_0 l)$ . We didn't compute higher-order terms, but it is reasonable to assume that the series are geometrical, at least approximately, in which case  $\lambda_{\text{eff}}$  can be approximated by  $\lambda_{\text{eff}} = \lambda_0 / (1 + b\lambda_0 l)$ . Using then this  $\lambda_{\text{eff}}$  instead of  $\lambda_0$  in (S7), we find

$$\chi = \frac{1}{1 - \lambda_{\text{eff}} l} \propto \frac{1}{1 - \lambda_0 l(1 - b)}. \quad (\text{S24})$$

The same result for  $\chi$  is obtained if we replace  $1 - 2l$  in the r.h.s. of (S11) by  $1 - b$ . The outcome then depends on the magnitude of  $b$ . For  $b > 1$ , consistent with our numerical result, a ferromagnetic susceptibility decreases as  $l$  increases. Then a ferromagnetic instability does not develop.

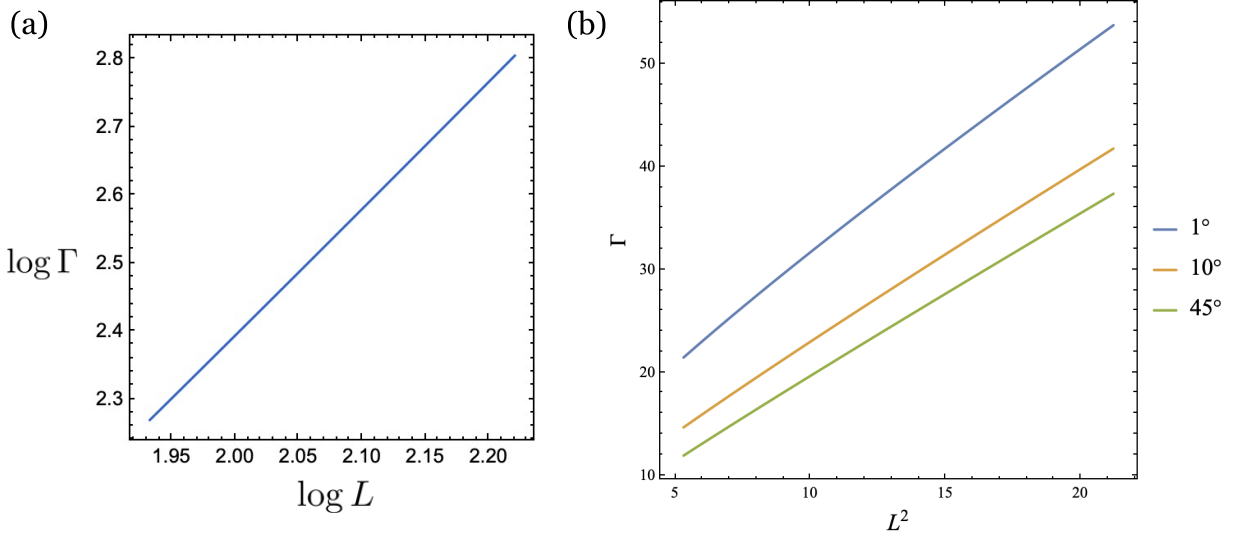


Figure S1. (a) The log-log plot of  $\Gamma$ , given by Eq. (S27) vs  $L = \log \frac{\Lambda}{|\mathbf{p}|}$ . The slope gives the value of the exponent of the power-law dependence of  $\Gamma$  on  $L$ . To a good accuracy,  $\Gamma = b' L^2$ . (b)  $\Gamma$  as a function of  $L^2$  for various polar angles of  $\mathbf{p}$  relative to the  $k_+$ -direction. For all angles,  $b'$  is in the range between 1.4 and 1.9.

The two-loop diagram in Fig. 2(c) can also be evaluated at zero temperature and regularized by a small but finite external momentum  $\mathbf{q}$ . In this case, the quantity we are computing is

$$\Gamma = \int \int \frac{d\omega d\Omega}{4\pi^2} \int \int \frac{dk_+ dk_-}{4\pi^2} \int \int \frac{dq_+ dq_-}{4\pi^2} G(q+p)^2 G(-k+q/2+p) G(k+q/2+p), \quad (\text{S25})$$

where  $q = (\mathbf{q}, \omega)$  and  $k = (\mathbf{k}, \Omega)$ . Integrating over frequencies, we get

$$\begin{aligned} \Gamma &= - \int \frac{dk_+ dk_- dq_+ dq_-}{(2\pi)^4} \left[ \theta(\epsilon_{k_+ + \frac{q_+}{2}}) - \theta(-\epsilon_{-k_+ + \frac{q_+}{2}}) \right] \frac{\theta(\epsilon_{-k_+ + \frac{q_+}{2}} + \epsilon_{k_+ + \frac{q_+}{2} + p}) - \theta(\epsilon_{q+p})}{(\epsilon_{q+p} - \epsilon_{k_+ + \frac{q_+}{2} + p} - \epsilon_{-k_+ + \frac{q_+}{2} + p})^2} \\ &= - \int \frac{dk_+ dk_- dq_+ dq_-}{(2\pi)^4} \left[ \theta\left(\left(k_+ + \frac{q_+}{2} + p_+\right)\left(k_- + \frac{q_-}{2} + p_-\right)\right) - \theta\left(-\left(k_+ - \frac{q_+}{2} - p_+\right)\left(k_- - \frac{q_-}{2} - p_-\right)\right) \right] \\ &\quad \times \frac{\theta(4k_+ k_- + (q_+ + 2p_+)(q_- + 2p_-)) - \theta((q_+ + p_+)(q_- + p_-))}{(4k_+ k_- - q_+ q_- + 2p_+ p_-)^2}, \end{aligned} \quad (\text{S26})$$

where  $\theta(x)$  is the step function. Without loss of generality, below we will consider  $p_+, p_- > 0$ . This restricts the range of integration over  $\mathbf{k}$  and  $\mathbf{q}$  to

$$\begin{aligned} \Gamma &= - \left( \int_{|\frac{q_+}{2} + p_+|}^{\Lambda} \int_{|\frac{q_-}{2} + p_-|}^{\Lambda} \frac{dk_+ dk_-}{4\pi^2} + \int_{-\Lambda}^{-|\frac{q_+}{2} + p_+|} \int_{-\Lambda}^{-|\frac{q_-}{2} + p_-|} \frac{dk_+ dk_-}{4\pi^2} \right) \\ &\quad \times \left( \int_{-p_+}^{\Lambda} \int_{-\Lambda}^{-p_-} \frac{dq_+ dq_-}{4\pi^2} + \int_{-\Lambda}^{-p_+} \int_{-p_-}^{\Lambda} \frac{dq_+ dq_-}{4\pi^2} \right) \frac{1}{(4k_+ k_- - q_+ q_- + 2p_+ p_-)^2} \\ &\quad - \left( \int_{|\frac{q_+}{2} + p_+|}^{\Lambda} \int_{-\Lambda}^{-|\frac{q_-}{2} + p_-|} \frac{dk_+ dk_-}{4\pi^2} + \int_{-\Lambda}^{-|\frac{q_+}{2} + p_+|} \int_{|\frac{q_-}{2} + p_-|}^{\Lambda} \frac{dk_+ dk_-}{4\pi^2} \right) \\ &\quad \times \left( \int_{-p_+}^{\Lambda} \int_{-p_-}^{\Lambda} \frac{dq_+ dq_-}{4\pi^2} + \int_{-\Lambda}^{-p_+} \int_{-\Lambda}^{-p_-} \frac{dq_+ dq_-}{4\pi^2} \right) \frac{1}{(4k_+ k_- - q_+ q_- + 2p_+ p_-)^2}, \end{aligned} \quad (\text{S27})$$

where  $\Lambda$  is a large momentum cutoff. We did the integration numerically and show the results in Fig. S1. In Fig. S1(a) we show that  $\Gamma \approx b' L^2$ , where  $L = \log \frac{\Lambda}{|\mathbf{p}|}$ . To estimate the value of  $b'$ , we note that the dispersion Eq. (4) breaks rotation symmetry, hence the value of  $\Gamma$  depends not only on the magnitude of  $\mathbf{p}$  but also on its direction relative to  $k_{\pm}$ . In Fig. S1(b) we plot  $\Gamma$  as a function of  $L^2$  for different polar angles of  $\mathbf{p}$ . We find that  $b'$  falls in the range between 1.4 and 1.9. We cannot get a more precise estimate of  $b'$  this way, but we emphasize that it is larger than one, in agreement with the result obtained using finite-temperature regularization.

**APPENDIX B. FERMIONIC SELF-ENERGY FOR AN EXTENDED VH POINT**

Equation (67) follows from the second order perturbation theory. It obeys the correct power counting  $Z_{b\mathbf{k}} = b^{-4\epsilon} Z_{\mathbf{k}}$  and recovers the  $\epsilon \rightarrow 0$  limit of Eq. (16). Let us sketch the main ingredients of the analysis. As before, we use Eq. (5) for the dispersion. To compute the self energy we need the dynamical polarization  $\Pi(\mathbf{q}, \omega_m)$ . Evaluating it at finite  $\epsilon$ , we obtain

$$\Pi(\mathbf{q}, \omega_m) = \frac{c}{A|\mathbf{q}|^{2\epsilon}} \left( 1 + b \frac{|\omega_m|}{A\Lambda|\mathbf{q}|^{1+2\epsilon}} \right), \quad (\text{S28})$$

where  $a, b$  are numbers of order unity. The minimum  $q_{\min}$ , up to which we can treat  $\Pi(\mathbf{q}, \omega_m)$  as a static, frequency-independent quantity is

$$q_{\min} \sim \left( \frac{|\omega_m|}{A\Lambda} \right)^{\frac{1}{1+2\epsilon}}. \quad (\text{S29})$$

We assume and verify that the relevant momenta that contribute to pairing are indeed larger than  $q_{\min}$ . The self-energy  $\Sigma_{\mathbf{k}}(\omega_m)$  is the convolution of  $\Pi$  with the fermionic propagator. Substituting this form of  $\Pi$ , we find after straightforward calculation that at  $\mathbf{k} = \mathbf{0}$ ,

$$\Sigma(\omega_m) \sim g\omega_m \left( \frac{A\Lambda^{2+2\epsilon}}{|\omega_m|} \right)^{\frac{4\epsilon}{1+2\epsilon}} \quad (\text{S30})$$

where  $c = O(1)$ . Using (S29) to relate frequencies and momenta and paying attention to the correct symmetry in momentum space, we recover Eq. (67).